Science of the Total Environment 775 (2021) 145669

Contents lists available at ScienceDirect

Science of the Total Environment

journal homepage: www.elsevier.com/locate/scitotenv

Uptake and effects of graphene oxide nanomaterials alone and in combination with polycyclic aromatic hydrocarbons in zebrafish

Ignacio Martínez-Álvarez [a,b], Karyn Le Menach [a], Marie-Hélène Devier [a], Iranzu Barbarin [c], Radmila Tomovska [c,d], Miren P. Cajaraville [b], Hélène Budzinski [a], Amaia Orbea [b,*]

[a] University of Bordeaux, EPOC-LPTC, UMR 5805 CNRS, F-33405 Talence Cedex, France
[b] CBET research group, Dept. of Zoology and Animal Cell Biology, Research Centre for Experimental Marine Biology and Biotechnology PiE and Science and Technology Faculty, University of the Basque Country (UPV/EHU), Sarriena z/g, E-48940 Leioa, Basque Country, Spain
[c] POLYMAT and University of the Basque Country UPV/EHU, Joxe Mari Korta Center - Avda. Tolosa, 72, 20018 San Sebastian, Spain
[d] IKERBASQUE, Basque Foundation of Science, Plaza Euskadi, 5, Bilbao 48009, Spain

HIGHLIGHTS

- Graphene oxide showed a high capacity to sorb PAHs depending on their hydrophobicity.
- Graphene oxide alone or with PAHs caused malformations in zebrafish embryos.
- Adult and embryo zebrafish ingested graphene oxide.
- Sublethal effects provoked by graphene oxide included neurotoxicity.
- Graphene oxide with sorbed PAHs caused oxidative stress in the gills.

GRAPHICAL ABSTRACT

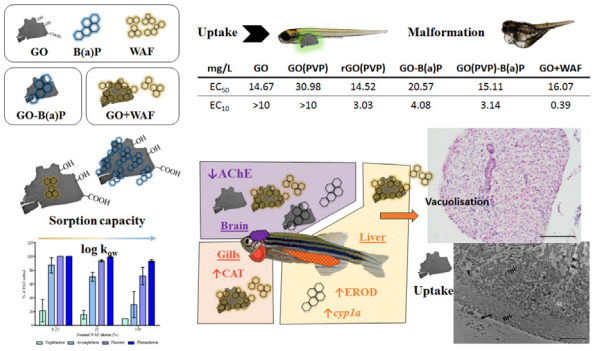

ARTICLE INFO

Article history:
Received 27 October 2020
Received in revised form 18 January 2021
Accepted 2 February 2021
Available online 6 February 2021

Editor: Daniel Wunderlin

Keywords:
Carbon based nanomaterials
Organic pollutants
Adsorption
Aquatic nanotoxicity

ABSTRACT

Because of its surface characteristics, once in the aquatic environment, graphene could act as a carrier of pollutants, such as polycyclic aromatic hydrocarbons (PAHs), to aquatic organisms. In this study we aimed to (1) assess the capacity of graphene oxide (GO) to sorb PAHs and (2) to evaluate the toxicity of GO alone and in combination with PAHs on zebrafish embryos and adults. GO showed a high sorption capacity for benzo(*a*)pyrene (B(*a*)P) (98% of B(*a*)P sorbed from a nominal concentration of 100 μg/L) and for other PAHs of the water accommodated fraction (WAF) of a naphthenic North Sea crude oil, depending on their log K_{ow} (95.7% of phenanthrene, 84.4% of fluorene and 51.5% of acenaphthene). In embryos exposed to different GO nanomaterials alone and with PAHs, no significant mortality was recorded for any treatment. Nevertheless, malformation rate increased significantly in embryos exposed to the highest concentrations (5 or 10 mg/L) of GO and reduced GO (rGO) alone and with sorbed B(*a*)P (GO-B(*a*)P). On the other hand, adults were exposed for 21 days to 2 mg/L of GO, GO-B(*a*)P and GO co-exposed with WAF (GO + WAF) and to 100 μg/L B(*a*)P. Fish exposed to GO presented GO in the intestine lumen and liver vacuolisation. Transcription level of genes related to cell cycle regulation and oxidative stress was not altered, but the slight up-regulation of *cyp1a* measured in fish exposed to B(*a*)P for 3 days resulted in a significantly increased EROD activity. Fish exposed to GO-B(*a*)P and to B(*a*)P for 3 days and to GO + WAF for 21 days showed significantly higher catalase activity in the gills than control fish. Significantly lower acetylcholinesterase activity, indicating neurotoxic effects, was also observed in all fish treated for 21 days. Results demonstrated the capacity of GO to carry PAHs and to exert sublethal effects in zebrafish.

* Corresponding author.
E-mail address: amaia.orbea@ehu.eus (A. Orbea).

https://doi.org/10.1016/j.scitotenv.2021.145669

1. Introduction

Graphene is a two-dimensional carbon nanomaterial (NM) formed by a single layer of carbon atoms densely packed into a benzene-ring structure (Chen et al., 2012). Large specific surface area, mechanical strength, and remarkable electric and thermal properties make graphene suitable for many new applications (Ghosal and Sarkar, 2018; Kinloch et al., 2018). The two dimensional single layer of carbon can be chemically functionalised to produce derivatives, such as graphene oxide (GO) and reduced graphene oxide (rGO). Functionalisation of graphene NMs confers them different characteristics, like higher dispersability and adaptability, and consequently allows additional applications (Wang et al., 2011). Due to the recent discovery of their potential applications, the scarce implementation in the market (Kong et al., 2019) and the analytical limitations, graphene NM concentrations in ecosystems are not reported yet. Nevertheless, predicted concentrations in aquatic ecosystems range from 0.001 to 1000 μg/L, which are similar to those reported for carbon nanotubes (De Marchi et al., 2018). Further the production of graphene NMs is expected to increase in the following years (Ciriminna et al., 2015).

The potential risk of graphene NMs for aquatic organisms is currently being investigated (De Marchi et al., 2018). The driving characteristics of their potential toxicity are surface properties (radicals and functional groups) that can change due to chemical reactions that occur in ecosystems, which could, in turn, alter the bioavailability of graphene NMs for organisms. Effects of graphene NMs are poorly understood, but evidence shows that graphene is able to go through cell membranes in invertebrates and fish (Lammel et al., 2014; Lammel and Navas, 2014; Katsumiti et al., 2017). In zebrafish, which has been reported as a suitable model organism for the assessment of graphene NMs toxicity (Dasmahapatra et al., 2019), GO has been shown to translocate from the water to the brains of parental and offspring fish, leading to remarkable neurotoxicity in the offspring (Hu et al., 2017). Several studies indicate that zebrafish larval stages are sensitive to graphene NMs toxicity (Liu et al., 2014; M. Chen et al., 2016; Ren et al., 2016; D'Amora et al., 2017; Soares et al., 2017; X. Zhang et al., 2017; Pecoraro et al., 2018). Acute effects have not been reported under exposure to high GO concentrations (1–100 mg/L), but several sublethal effects including development delay, hatching rate alterations, neurotoxic effects, oxidative stress, cardiac alterations and locomotor alterations have been observed (M. Chen et al., 2016; D'Amora et al., 2017; Soares et al., 2017). In embryos exposed to environmental concentrations of GO (0.01–100 μg/L) sublethal effects, such as oxidative stress, skeletal developmental delay and alterations in the nervous system have been reported even at the lowest exposure concentration (0.01 μg/L) (Ren et al., 2016; X. Zhang et al., 2017). Toxicity of graphene NMs has also been tested in adult zebrafish (Y. Chen et al., 2016; Souza et al., 2017). Exposure to 1–50 mg/L GO for 14 days provoked oxidative stress at short term (4 days) and induction of tissue damage, such as increase of liver vacuolisation, at all the exposure concentrations tested (Y. Chen et al., 2016). Zebrafish exposed to GO (2–20 mg/L) showed similar effects with alterations in the liver (vacuolisation and pycnotic nuclei) and in the gills, such as lamellar fusion and clubbed tips (Souza et al., 2017).

One characteristic of graphene NMs that could modulate the previously described effects on aquatic organisms is their ability to sorb organic compounds, especially polycyclic aromatic hydrocarbons (PAHs). Due to the surface hydrophobicity, surface area and micropore volume, graphene NMs display a high PAH sorption capacity (Apul et al., 2013; Ji et al., 2013; Pei et al., 2013; Wang et al., 2014; Zhao et al., 2014) based on hydrophobic interactions (π–π interactions). In addition, graphene NMs can sorb pollutants by other interaction types, such as ion exchange or hydrogen bonding thanks to the presence of different functional groups (epoxy groups, C—O—C; hydroxyl groups, C═O; carboxylic groups, C—OOH) (Wang and Chen, 2015; Smith and Rodrigues, 2015; Yan et al., 2015). Based on this characteristic, carbon NMs are being investigated as remediation materials for water treatment (Tabish et al., 2018; Baig et al., 2019). One example of this application is the use of 3D materials containing NMs such as graphene for remediation of oil spill scenarios (mainly PAHs) (Niu et al., 2014). These uses could represent an additional source of graphene into aquatic ecosystems that could modulate the availability of PAHs for aquatic organisms (Naasz et al., 2018). To the best of our knowledge, only two studies have addressed the potential "Trojan horse effect" of graphene NMs contaminated with persistent organic pollutants to zebrafish (J. Yang et al., 2019; Liu et al., 2020). Mortality increase and hatching delay were reported in zebrafish embryos exposed to irradiated graphene aerogel combined with naphthalene (Liu et al., 2020). In contrast, GO reduced the bioavailability of the endocrine disruptor bisphenol A to early stages of zebrafish embryos (J. Yang et al., 2019). Other carbon NMs were previously studied for potential transfer of PAHs to zebrafish (Falconer et al., 2015; Della Torre et al., 2017). Carbon nanopowder promoted the bioaccumulation of benzo(*a*)pyrene (B(*a*)P), enhanced the cytotoxicity, and the number of necrotic cells in zebrafish embryos (Della Torre et al., 2017). On the contrary, carbon nanotubes (CNTs) in combination with phenanthrene increased the survival rate of zebrafish embryos compared to phenanthrene alone, showing the capacity of some carbon NMs to reduce the availability of PAHs to zebrafish (Falconer et al., 2015). Although some studies have already addressed this issue, work is still to be done to elucidate the role of graphene NMs to affect and modulate PAH availability and effects to aquatic organisms. The aims of the present work were: (1) to assess the sorption capacity of GO NMs for a model high molecular weight pyrolytic PAH such as B(*a*)P and for an environmentally relevant mixture of petrogenic PAHs from the water accommodated fraction (WAF) of a crude oil; (2) to assess the uptake and potential acute toxicity of GO NMs alone or in combination with PAHs to zebrafish embryos; (3) to evaluate the sublethal toxicity of GO alone and in combination with PAHs to adult zebrafish.

In order to accomplish these objectives, three GO NMs were incubated in three different concentrations of B(*a*)P and the corresponding sorption isotherms were calculated. Additionally, GO sorption capacity was also assessed for the PAHs of the WAF of a crude oil by incubating GO in three WAF dilutions and calculating the sorption isotherms. The effect of the PAH contamination on the graphene platelet aggregation was evaluated by transmission electron microscopy and atomic force microscopy. The acute toxicity of GO NMs alone and in combination with PAHs was tested in developing zebrafish embryos by exposing them up to five days post-fertilisation. Survival and hatching rates, hatching delay and increased malformation prevalence were scored as indicators of acute toxicity. Fluorescent reduced GO was used to track GO uptake in embryos. Based on the results obtained in the sorption assays, an in vivo exposure experiment with adult zebrafish was designed. Individuals were exposed for up to 21 days to GO alone and with sorbed B(*a*)P and to B(*a*)P alone at a concentration equivalent to that estimated to be sorbed to GO. Due to the low PAH concentration of the produced WAF, adult fish were also coexposed to GO and diluted WAF. The effects on these individuals were studied using a set of molecular (gene transcription) and biochemical markers (enzyme activities) along with the histopathological assessment of the gill and liver tissues. GO and PAH accumulation in fish as well as concentration in exposure media was monitored.

2. Materials and methods

2.1. Nanomaterials and chemicals

GO was originally purchased from Graphenea (San Sebastian, Spain) in form of a stable suspension. According to manufacturer's information, nanoplatelets showed lateral dimensions ranging from 500 nm to few microns and thickness < 2 nm. Oxygen content was about 40% wt. Part of the GO suspension was stabilised with 2% of poly N-vynil-2-

pirrolidone (PVP, Sigma-Aldrich, St. Louis, MO, USA) to produce GO(PVP). After stabilisation GO(PVP) samples were dialysed (12–14,000 Da spectral/Por® membranes, Spectrumlabs (Piraeus, Greece)), in order to remove the excess of PVP, until samples reached a neutral pH. To obtain reduced rGO, GO was chemically reduced by hydrazine monohydrate (5:1) at 60 °C for 2 h in the presence of PVP as stabilising agent. Afterwards, rGO samples were also dialysed (12–14,000 Da spectral/Por® membranes, Spectrumlabs (Piraeus, Greece)), in order to remove secondary products of the reduction of GO and excess of PVP. Final rGO suspensions contained 2% PVP (rGO (PVP)). Fluorescent rGO (Fl-rGO) was produced from GO originally purchased to Graphene Supermarket (Graphene Laboratories Inc., Ronkonkoma, NY, USA). Fluorescent GO was reduced in the same way as GO. After reduction and fluorescent labelling with fluorescein, the Fl-rGO was dialysed as previously explained and was stabilised with 2% of PVP.

Benzo(*a*)pyrene (B(*a*)P, $C_{20}H_{12}$, purity ≥ 96%), its internal standard (B(*a*)P d_{12}), other deuterated PAHs (naphthalene d_8, acenaphthylene d_{10}, acenaphthene d_{10}, fluorene d_{10}, anthracene d_{10}, phenanthrene d_{10}, fluoranthene d_{10}, pyrene d_{10}, benzo(*a*)anthracene d_{12}, chrysene d_{12}, benzo(*e*)pyrene d_{12}, perylene d_{12}, benzo(*b*)fluoranthene d_{12}, benzo(*k*)fluoranthene d_{12}, indeno(1,2,3-*cd*)pyrene d_{12}, benzo(*ghi*) perylene d_{12} and dibenz(*a*,*h*)anthracene d_{14}) and dimethyl sulfoxide (DMSO, purity ≥ 96%) were purchased from Sigma-Aldrich. The naphthenic North Sea (NNS) crude oil was provided by Driftslaboratoriet Mongstad, Equinor (former Statoil; Statoil, 2011). The oil was a very light naphthenic crude oil, with a density of 0.845 g/cc at 15 °C and pour point at −15 °C, rich in branched and cyclic saturated hydrocarbons, little wax content, poor thermal and oxidative stability and high octane content (Statoil, 2011).

2.2. PAH sorption to GO NMs

B(*a*)P was firstly dissolved in 100% DMSO at a concentration of 10 g/L. Successive dilutions were made in pure DMSO to obtain B(*a*)P stocks of 0.01, 0.1 and 1 g/L. From each of them, a 1:10,000 dilution in conditioned water (600 μS/cm, 7–7.5 pH) was prepared to obtain the nominal B(*a*)P concentrations that were used in the sorption experiments: 1, 10 and 100 μg/L (0.01% DMSO (*v*/v)). WAF was prepared, based on Singer et al. (2000), in a glass bottle of 150 mL filled with conditioned water and NNS oil (1/50, NNS to conditioned water). The bottle was wrapped with aluminium foil and placed in a magnetic stirrer (IKA®-Werke GmbH & Co. KG, Staufen, Germany) at 800 rpm without vortexing and 21 °C. After 40 h, the aqueous phase was collected in a clean glass bottle avoiding taking oil droplets. 100% WAF samples were stored at −20 °C until chemical analysis.

For sorption experiments, 50 mg/L GO, GO(PVP) or rGO(PVP) were incubated in triplicate for 24 h in capped aluminium-wrapped glass vials containing 10 mL of 1, 10 and 100 μg/L of B(*a*)P or of 6.25, 25 and 100% WAF (*v*/v). Vials containing the corresponding PAH solutions without graphene were processed in parallel to monitor potential PAH loss due to degradation, sorption onto the vial walls or other factors during the experimental procedure. Vials were kept in an orbital shaker (M1000 VWR, Thorofare, USA) at 300 rpm in darkness in a temperature-controlled room (21 ± 1 °C). After incubation, samples were centrifuged (Hettich Universal 32R centrifuge, Tuttlingen, Germany) at 9509 g for 30 min. Recovery of GO NMs after centrifugation was assessed by spectrophotometry at 230 nm (Fig. S1). Then, supernatants were diluted up to 1 μg/L according to nominal PAH concentration with deionised water in 10 mL glass solid phase micro extraction (SPME) vials. The 18 PAHs (16 priority PAHs selected by the US EPA (Environmental Protection Agency) and 2 additional parent PAHs (benzo (*e*)pyrene and perylene)) were quantified by isotopic dilution using deuterated standards added prior the extraction to calculate raw recoveries for surrogate internal standards. The 18 deuterated PAHs were dissolved separately in ethanol at a concentration of 20 ng/g for SPME extraction. A blank analysis was carried out to ensure the absence of contamination prior and during analysis. SPME consisted in a heating process at 40 °C with 35 min stirring period at 250 rpm of the polydimethylsiloxane fibre (100 μm PDMS, Supelco, Sigma-Aldrich, Johannesburg, South Africa). After extraction, the fibre was thermally desorbed into the gas chromatography/mass spectrometry (GC/MS) system (Agilent GC 7890A/Agilent MSD 5975C, Agilent Technology, California) for 10 min at 280 °C. Limits of detection and quantification (L.Q.) were defined at which the signal to noise ratio was >3 and 10, respectively, in spiked water samples. The GC/MS instrumentation, quality assurance and controls (L.Q., control charts and percentage of PAH recovery in control samples) that were carried out are reported on the Supporting Information (Tables S1 and S2).

Based on the PAH concentration measured in the aqueous phase, sorption of PAHs to GO was indirectly calculated. Values of sorption were expressed as Q_e (μg/g), which is the sorption concentration of PAH to GO at equilibrium and it was calculated as follows (Eq. (1)):

$$Q_e = \frac{(C_0 - C_e)\,V}{M} \tag{1}$$

where C_e (μg/L) is the equilibrium concentration in the aqueous phase, C_0 (μg/L) is the average PAH concentration of the control sample after centrifugation, V (L) is the medium volume and M (g) is the GO mass. When the 100% of a given PAH was sorbed to GO, L.Q. value of that PAH was used as C_e. In order to evaluate PAH sorption to GO, the linear and Freundlich sorption isotherm models were applied. Linear model (Eq. (2)) was applied from Q_e and C_e values obtained for the sorption capacity of GO for PAHs:

$$Q_e = k_d C_e \tag{2}$$

where K_d (L/g) is the partition coefficient of the PAH between GO and the aqueous phase.

Freundlich model (Eq. (3)) was used for parameter acquisition:

$$Q_f = k_f {C_e}^N \tag{3}$$

where K_f [(μg/g)/(μg/L)^N] is the Freundlich affinity coefficient, and N is the exponential coefficient.

2.3. Characterisation of the GO NMs

GO-B(*a*)P and GO(PVP)-B(*a*)P were prepared as described above by incubating GO and GO(PVP) for 24 h in 100 μg/L B(*a*)P (0.01% DMSO). GO, GO(PVP), rGO(PVP) and GO-B(*a*)P and GO(PVP)-B(*a*)P were diluted in conditioned water at a concentration of 100 mg/L for transmission electron microscopy (TEM) and at 10 mg/L for atomic force microscopy (AFM). For TEM, one drop of each NM dispersion was placed over a 150 mesh copper grid previously covered with Formvar® (Sigma-Aldrich) and dried at 35 °C. Micrographs were taken using a high resolution JEOL 2000 microscope (JEOL Co., Tokyo, Japan) operated at 80 kV. For atomic force microscopy (AFM) each NM dispersion was placed in grade V mica disks and deposited by spin coating. AFM measurements were performed using Dimension ICON AFM (Bruker Corporation, Massachusetts, USA) and micrographs were obtained in the intermittent-contact (tapping) mode (320 kHz) with a TESP-V2 cantilever with a spring constant of 40 N/m. Three representative platelets were taken from each sample to measure their length and thickness using the NanoScope Analysis 1.9 software (Bruker Corporation, Santa Barbara, USA).

2.4. Zebrafish maintenance and egg production

The zebrafish (wild type AB Tübingen) stock was maintained in a temperature-controlled room at 28 °C with a 14-hour light/10-hour dark cycle in 100 L tanks provided with mechanic and biological filters

following standard protocols for zebrafish culture. Conditioned water was prepared from deionised water and commercial salt (SERA, Heinsberg, Germany). Fish were fed with Vipagran baby (Sera) and brine shrimp larvae (Artemia Koral GmbH, Nürnberg, Germany) twice per day.

Breeding female fish were selected and maintained separately in fish breeding nets inside the same tanks in order to avoid continuous spawning. The day before the assay, one female and two male zebrafish were placed separately in the same breeding tramp, which had previously been located in a 2 L tank containing conditioned water. Fish were left overnight and, just before the light switched on, the separation barrier was removed. The fertilised eggs were collected in a Petri dish with the help of a Pasteur pipette. The eggs selected as viable under a stereoscopic microscope (Nikon smz800, Kanagawa, Japan) were transferred to the exposure microplates.

2.5. Embryo toxicity test

For the embryo toxicity tests, GO NMs alone, GO NMs with sorbed PAHs and B(*a*)P solutions were diluted in embryo water (600–800 μS/cm, pH 6.5–6.8, Brand et al., 2002) at the desired nominal concentrations: 0.1, 0.5, 1, 5 and 10 mg/L GO or B(*a*)P. GO NMs with sorbed B(*a*)P were prepared as described above by incubating GO and GO (PVP) in 100 μg/L B(*a*)P (0.01% DMSO) for 24 h followed by centrifugation to separate GO from the incubation medium. In the case of GO with sorbed PAHs from WAF, GO was incubated in 100% WAF for 24 h and, then, diluted at the above mentioned GO concentrations. Thus, in the case of GO + WAF, co-exposure to adsorbed and soluble PAHs took place. The toxicity tests were carried out in covered 24-well polystyrene microplates placing one embryo per well in 2 mL of test solution based on the OECD guideline TG236 (OECD TG236, 2013). In each microplate, two different concentrations were tested (10 embryos per concentration). In the remaining wells, four control embryos were placed in embryo water. For each compound three replicates were prepared, resulting in 30 embryos exposed to each concentration and 36 control embryos. Embryos were exposed up to 120 hours post fertilisation (hpf). The exposure medium was not renewed during the 5 day exposure period. The test was considered as valid only when the survival of the control group of each replicate was ≥90%. Daily and up to the end of the test, embryos were examined to determine survival rate (as the percentage of alive embryos at 120 hpf), hatching time (as the time that embryos needed to hatch) and malformation prevalence (as the percentage of malformed embryos over surviving embryos at 120 h). Normal embryo morphology and malformation identification were based on Fako and Furgeson (2009). Developmental abnormalities scored as malformations were spinal cord flexure, caudal fin alteration, tail malformation, pericardial edema, yolk sac edema, eye abnormality and stunted body. Malformations were recorded and photographed under a stereoscopic microscope (Nikon AZ100, Kanagawa, Japan).

Groups of 10 embryos were exposed in Petri dishes for 120 h to fluorescent rGO (1 and 10 mg/L) in order to analyse the uptake and distribution in the embryo body. At 120 h of exposure the individuals were observed under a fluorescence stereoscopic microscope (Nikon AZ100). For the micrographs, the organisms were anesthetised with benzocaine (200 mg/L).

2.6. Waterborne exposure of adult zebrafish

The experimental procedure described herein was approved by the Ethics Committee in Animal Experimentation of the UPV/EHU (NoRefCEID: M20/2018/232) according to the current regulations. Adult fish more than 7 months old were placed in 35 L aquaria with conditioned water. Fish were exposed to 2 mg/L of GO alone, 2 mg/L of GO with sorbed B(*a*)P, 2 mg/L of GO + WAF and to 100 μg/L B(*a*)P alone for 21 days. Water and pollutants were renewed every 3 days by changing 5/7 of the tank volume (25 L from a total of 35 L). This allowed maintaining water quality parameters along the whole experiment without the need of biological filters that could interfere with the exposure. An unexposed control group was run in parallel in identical experimental conditions. Fish were feed with live brine shrimp larvae twice per day. Samples were taken after 3 and 21 days of exposure after euthanasia by overdose of anaesthetic (200 mg/L benzocaine).

For the preparation of the exposure media containing GO with sorbed PAHs, the GO mass/PAH mass ratio used in the sorption experiments was maintained. For the initial dose, 70 mg GO were incubated for 24 h in 100 mL of 1400 μg/L of B(*a*)P prepared in MilliQ water. For the following doses, 50 mg GO were incubated in 71 mL of 1400 μg/L of B(*a*)P. After centrifugation, the pellet was resuspended with conditioned water and added to the 35 L exposure tanks, resulting in a nominal exposure concentration of 2 mg/L of GO-B(*a*)P. The concentration used in the group exposed to B(*a*)P alone was based on the results of the sorption experiments. In the case of GO incubated in 100 μg/L B(*a*)P, 96.7% B(*a*)P was lost from the aqueous phase. Thus, considering that almost all B(*a*)P was sorbed onto GO nanoplatelets, this B(*a*)P incubation concentration was used for adult zebrafish exposure.

Due to the low PAH concentration of the produced WAF, in the case of GO + WAF, a co-exposure scenario was established. For this, for the initial dose, 70 mg GO were incubated in 1.4 L of 100% WAF, prepared as described before, for 24 h. As this WAF volume was too high for further centrifugation, this mixture was added to the exposure tanks to achieve a nominal concentration of 2 mg/L GO and 4% WAF (co-exposure), considering that the most hydrophobic PAHs from WAF are highly sorbed by GO while less hydrophobic PAHs are more volatile. For the following doses, 50 mg of GO were incubated for 24 h in 1 L of 100% WAF.

2.6.1. Monitoring of GO and PAH concentrations in water and PAH bioaccumulation in adult zebrafish

In order to monitor the GO concentration in exposure tanks, water samples were taken in triplicate in glass vials from tanks containing GO (GO, GO + WAF and GO-B(*a*)P) after 5 min, 4 h, 24 h, 48 h and 72 h of the 3rd and 7th doses. GO was quantified by UV/Vis spectrophotometry at 230 nm using a microplate reader (Multiskan Spectrum, Thermo Fisher Scientific Oy, Vantaa, Finland). Absorbance values of each sample were converted into GO concentrations using a GO calibration curve (0.5–10 mg/L) prepared in conditioned water. For PAH quantification in the exposure media, water samples were taken in triplicate in glass vials from the PAHs containing groups (GO + WAF, GO-B(*a*)P and B(*a*)P) and from the control group after 5 min, 4 h, 8 h, 24 h, 48 h and 72 h of the initial dose. PAH quantification was performed as described above for the sorption experiments.

After 21 days of exposure, 20 fish per experimental group (control, GO + WAF, GO-B(*a*)P and B(*a*)P) were collected and grouped in 4 pools of 5 fish of similar weight (≈1 g wet weight). Samples were immediately frozen in liquid nitrogen and stored at −80 °C until analysis. Concentrations of PAHs in fish tissues were analysed using established analytical methods (Baumard et al., 1997) as described in detail in Turja et al. (2013, 2014). Samples were freeze dried (Power Dry LL3000, ThermoFisher Scientific) before being grinded in IKA tube mill (ThermoFisher Scientific). PAHs were extracted from 0.2 g of dry weight samples by microwave-assisted extraction (Start E, Milestone, Leutkirch, Germany) using dichloromethane (5 min at 900 W and 5 min at 500 W 70 °C). PAHs were quantified by isotopic dilution using deuterated internal standards added prior the extraction according to a protocol adapted from Baumard et al. (1997, 1999). After extraction, dichloromethane was concentrated to 500 μL using a Vacuum Evaporation System (Rapidvap Labconco, Kansas city, USA). The organic extracts followed a purification step through alumina and silica microcolumns in order to remove macromolecules and polar molecules to avoid interference on PAH quantification. First, the extracts were passed through an alumina column by dichloromethane elution. Extracts were reconcentrated with gas nitrogen and, then, passed through a silica

column. The aliphatic fraction was eluted with pentane and discarded, followed by PAH fraction elution with a first elution using a mix of pentane/dichloromethane (65/35, *v*/v) and second elution using dichloromethane. The final extracts were reconcentrated again with gas nitrogen in 150 μL isooctane and analysed by GC–MS. Syringe deuterated PAHs (pyrene d_{10} and benzo(*b*)fluoranthene d_{12}) were added prior the injection to calculate raw recoveries for surrogate internal standards (Table S3). All steps of the analytical protocol were validated in terms of reproducibility and accuracy; procedural blanks were systematically checked and certified reference mussel tissues (2974a NIST for PAHs,) were analysed together with the actual samples. The obtained recoveries ranged between 70 and 120% with coefficient of variation <20%. The detection limits of individual compounds in mussel tissues were in the range 0.1–1 ng/g dry weight for all PAHs.

2.6.2. Subcellular localisation of GO: transmission electron microscopy (TEM) analysis

Gills, liver and intestine from adult control fish and fish exposed to GO for 21 days were dissected and fixed for 1 h at 4 °C in sodium cacodilate (Sigma-Aldrich) buffer 0.1 M, pH 7.2 containing 2.5% glutaraldehyde (Panreac, Barcelona, Spain). Zebrafish tissue samples were treated and processed as described in Lacave et al. (2018). Ultrathin sections of 50 nm in thickness were cut using a Reichert Ultracut S ultramicrotome (Leica Microsystems, Wetzlar, Germany). Sections were picked up in 150 mesh copper grids, contrasted with 1% uranyl acetate (Fluka, Steinheim, Germany) for 3 min and with 0.3% lead citrate (Fluka) for 4 min and, finally, examined and photographed using a Hitachi HT7700 transmission electron microscope (Tokyo, Japan) at 60 kV.

2.6.3. Analysis of gene transcription levels

The liver of 15 adult male zebrafish per experimental group after 3 and 21 days of exposure were dissected, placed in cryovials with RNA later® (Sigma-Aldrich), frozen in liquid nitrogen and stored at −80 °C. Analysis of the transcription levels of target genes was done in pools of three livers resulting in five biological replicates per experimental group and exposure time. The analysed genes were: cytochrome P450 1A1 (*cyp1a*, ID: Dr03112441_m1) and glutathione S-transferase pi 1 (*gstp1*, ID: Dr03118992_g1) as genes related with biotransformation of organic compounds; catalase (*cat*, ID: Dr03099094_m1), superoxide dismutase 1 (*sod1*, ID: Dr03074068_g1) and glutathione peroxidase 1a (*gpx1a*, *ID*: Dr03071768_m1) as genes related with oxidative stress; and tumour suppressor protein 53 (*tp53*, ID: Dr03112086_m1) as gene related with cell cycle regulation. Ribosomal protein S18 (*rps18*, ID: Dr03144509_ml) was used as housekeeping gene. Taqman® probes were purchased from ThermoFisher Scientific. RNA extraction was carried out by homogenisation of the tissues in cold TRIzol® using an electric disperser (PELLET PESTLE-Cordless Motor, Kimble Kontes, U.S.A.). RNA was measured for integrity and purity before cDNA synthesis. 3 μg of total RNA were retrotranscribed using the Affinity Script Multiple Temperature cDNA synthesis Kit (Agilent Technologies) following manufacturer's conditions in a 2720 Thermal Cycler (ThermoFisher Scientific). qPCRs were run in a 7300 Applied Biosystems thermocycler (ThermoFisher Scientific). A dilution 1:5 of cDNA was done for each target gene. A final volume of 2.5 μL cDNA sample and 22.5 μL mix TaqMan® reaction (12.5 μL master mix + 1.25 μL primer probe + 8.75 μL RNase free water) was used. Relative transcription levels were calculated based on the $2^{-\Delta\Delta ct}$ method (Livak and Schmittgen, 2001) using the mean value of the corresponding control group at each exposure time as calibrator and *rps18* transcription levels as reference gene. *rps18* transcription levels presented a coefficient of variation of 2.34% among all the samples. Results of transcription levels are represented as $RQ = \log_2 (2^{-\Delta\Delta CT})$.

2.6.4. Analysis of biochemical biomarkers

Liver, gills and brains collected from 15 adult female fish per experimental group after 3 and 21 days of exposure were dissected, immediately frozen in liquid nitrogen and kept into cryovials at −80 °C until analysis. Pools of three livers, gills or brains were homogenised in 300 μL cold homogenisation buffer (50 mM potassium phosphate buffer containing 1 mM ethylenediaminetetraacetic acid, 0.5 mM dithiothreitol and 0.4 mM phenylmethylsulfonyl fluoride, pH 7.5) for 15 s on ice using an electric disperser resulting in 5 samples per treatment. The homogenates were centrifuged at 10,000*g* and 4 °C for 15 min (Eppendorf 5415R refrigerated centrifuge, Eppendorf AG, Hamburg, Germany). Supernatants were carefully transferred to new micro test tubes, aliquoted on ice for different enzymatic and protein measurements and stored at −80 °C until further use. Four biochemical biomarkers were analysed: 7-ethoxyresorufin-O-deethylase (EROD) activity, glutathione-S-transferase (GST) activity and catalase (CAT) activity in gills and liver and acetylcholinesterase (AChE) activity in brains.

EROD activity in liver and gill tissues was measured according to Kennedy and Jones (1994). Briefly, 20 μL of samples (in triplicate) and of resorufin standards were preincubated in 200 μL of 7-ethoxyresorufin (0.5 μM) for 10 min at room temperature. 20 μL NADPH (1 mM) were added to each well to activate the deethylation of 7-ethoxyresorufin to fluorescent resorufin. Resorufin was measured at 540/590 nm excitation/emission wavelengths for 25 min in 30 s intervals in a microplate reader (FLx800, Bio-Tek Instruments, INC, Winooski, U.S.A.). The standard curve was prepared using a resorufin concentration range from 0.004 to 1 μM on Tris-KCl buffer (pH 7.4). EROD activity was expressed as nmol of resorufin produced per min and mg protein.

GST activity in liver and gill tissues was measured according to Habig and Jakoby (1981) with the modifications done by Velki et al. (2017) for 96-well microplates. The conjugation of glutathione (GSH) was assessed by adding 12 μL of sample, in quadruplicate, to 180 μL of 1 mM 1-chloro-2,4-dinitrobenzene and 50 μL of reduced GSH (25 mM). Activity was assessed through the increase of absorbance due to the conjugation of GSH at 340 nm for 15 min in 10 s intervals in a microplate reader (Multiskan Spectrum). Values of sample activity were validated when they fulfilled two criteria: a linear increase of absorbance ($R^2 \geq 0.98$) and a minimum increase of absorbance over time ($\Delta t_{3min} \geq 0.1$). GST activity was expressed as nmol of conjugated GSH per min and mg protein.

CAT activity in liver and gill tissues was assayed according to Aebi (1984) adapted to UV 96-well microplates (Thermo Fisher Scientific). 5 μL of each sample, in quadruplicate, were added to 295 μL of 20.28 mM H_2O_2 in potassium phosphate buffer (0.5 mM, pH 7). Consumption of H_2O_2 by catalase was monitored at 240 nm for 5 min in 5 s intervals in the same microplate reader. The standard curve of H_2O_2 was prepared at a concentration range from 0.4 to 20.28 mM. CAT activity was expressed as μmol H_2O_2 consumption per min and mg protein.

AChE activity in brain tissues was measured according to the initial protocol established by Ellman et al. (1961) with modifications according to Velki et al. (2017) for 96-well microplates. The hydrolysis of acetylthiocoline (7.52 mM) was evaluated in a final volume of 207.5 μL of 86.7 mM of potassium phosphate buffer (pH 7.2) and 7.52 mM of 5,5′-dithiobis-(2-nitrobenzoic acid). 7.5 μL of sample were used in triplicate. Activity was measured by the increase of absorbance at 412 nm for 25 min in 10 s intervals using the same microplate reader. Values of sample activity were validated when they fulfilled the criteria used for GST. AChE was expressed as nmol of acetylcholine hydrolysed per min and mg of protein. Protein concentration was measured using the Bio-Rad DC protein assay (Bio-Rad Laboratories Inc., Hercules, California, USA) based on Lowry's method following instructions of the manufacturer.

2.6.5. Histopathology

Visceral mass and gills were dissected from 10 adult zebrafish per experimental group after 3 and 21 days of exposure. The collected tissues were placed in histological cassettes and immersed in neutral

buffered formalin (4% formaldehyde) for 13 h at 4 °C. Then, samples were dehydrated in a graded ethanol series (70%, 96% and 100% ethanol) and immersed in xylene at room temperature by an Automatic Tissue Processor MTP (SLEE medical GmbH, Mainz, Germany) for a total of 11 h before embedding in paraffin at 60 °C. Paraffin blocks were done using plastic moulds. 5 μm sections were cut in a RM2125RT microtome (Leica Microsystems). Afterwards, sections were stained with haematoxylin/eosin in an Auto Stainer XL (Leica Microsystems) and mounted in DPX (Sigma-Aldrich) by means of a CV5030 Robotic Coverslipper (Leica Microsystems). After staining and mounting, samples were examined and photographed using a BX51 light microscope (Olympus, Tokyo, Japan).

2.7. Data analysis and statistics

Data on survival and malformations for zebrafish embryos were analysed by binomial logistic regression (Lacave et al., 2017; Orbea et al., 2017). Odd ratios were calculated in order to estimate and to compare the risk associated with the exposure to the GO NMs alone and in combination with PAHs. EC_{50} and EC_{10} values were calculated using a Probit model. For binomial logistic regression and Probit model, R package (R Foundation for Statistical Computing, Vienna, Austria) was used. Data on hatching time of zebrafish embryos followed a Normal distribution, therefore data were analysed by one-way ANOVA followed by the Tukey's post hoc test. Data obtained from adult zebrafish were tested for normality (Kolmogorov-Smirnov test) and homogeneity of variances (Bartlett test) using the GraphPad Prism version 5.00 for Windows (GraphPad Software, La Jolla, California, USA). Data following a normal distribution were analysed by one-way ANOVA followed by the Tukey's post hoc test, otherwise the non-parametric Kruskal-Wallis test was applied followed by the Dunn's post hoc test. Prevalence of histopathological alterations in gill and liver tissues was analysed by Fisher's exact test. In all cases, statistical significance was established at $p < 0.05$.

3. Results

3.1. PAH sorption to GO NMs

B(*a*)P recovery after centrifugation of the control samples of GO experiments was 45.26% of the 0.69 ± 0.12 μg/L of B(*a*)P measured in the samples prepared at a nominal concentration of 1 μg/L (Table S2). As shown in Fig. 1A, at this incubation concentration, 100% of the B(*a*)P was sorbed to GO. In the nominal B(*a*)P incubation concentrations of 10 and 100 μg/L, measured B(*a*)P concentrations were 6.23 ± 0.23 μg/L and 118.5 ± 4.78 μg/L and recovery values were 69.79 and 76.91%, respectively. At these concentrations, B(*a*)P sorption percentages were 87.2 ± 2.1% and 96.68 ± 0.5%, respectively. In the case of GO(PVP), 96.96 ± 5.26% of B(*a*)P was sorbed from a measured concentration of 0.81 ± 0.08 μg/L (nominal concentration 1 μg/L). At nominal B(*a*)P concentrations of 10 and 100 μg/L, measured B(*a*)P concentration values were 7.11 ± 0.28 μg/L and 149.8 ± 1.65 μg/L and the sorption percentages 90.44 ± 2.3% and 96.44 ± 0.3%, respectively. Results could not be obtained for rGO(PVP) due to the remaining rGO(PVP) platelets in the supernatant after centrifugation, which interfered with the SPME/GC/MS analysis resulting in no signal for PAHs or deuterated PAHs.

The sorption isotherms of B(*a*)P to GO and GO(PVP) are represented in Fig. 1B. The corresponding constants and parameters obtained from Linear and Freundlich models for GO and GO(PVP) are shown in Table 1. Regarding the Linear model, values of the distribution coefficient (K_d) for B(*a*)P sorption to GO and to GO(PVP) were 756.58 L/g and 575.05 L/g, respectively. Values of correlation coefficient (R^2) for the Linear model (0.88 and 0.91, respectively) were similar to those obtained for the Freundlich model (0.83 for GO and 0.89 for GO(PVP)). The Freundlich affinity coefficient (K_f) was higher for B(*a*)P sorption to GO (665.47 $(\mu g/g)/(L/\mu g)^N$) than to GO(PVP) (357.78 $(\mu g/g)/(L/\mu g)^N$). In addition, the Freundlich "N" cooperation factor was similar for B(*a*)P sorption to GO or GO(PVP), 1.59 and 1.52, respectively.

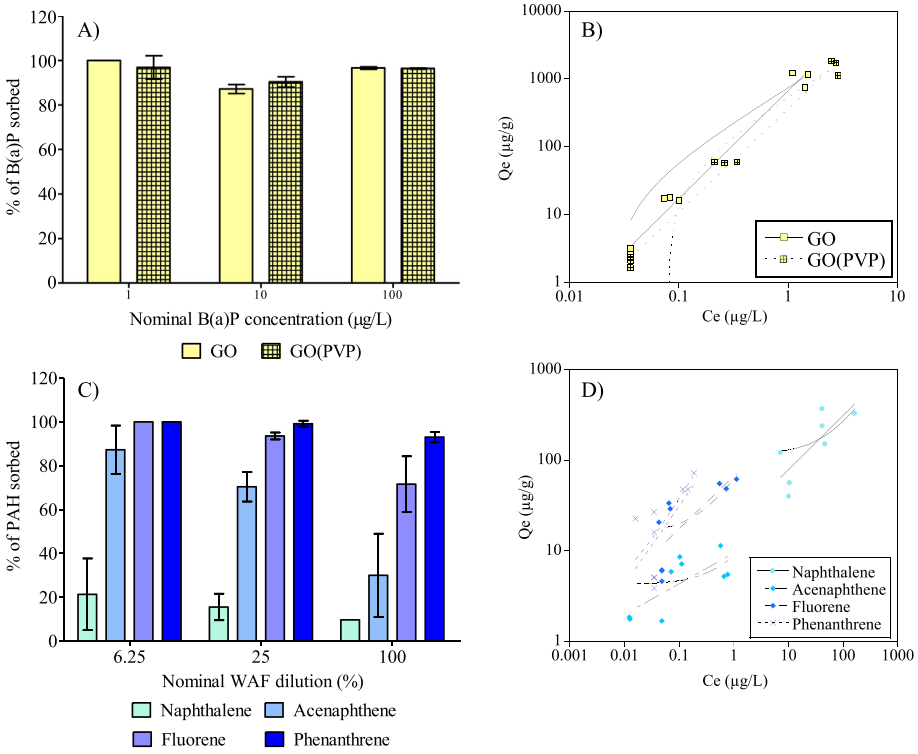

Fig. 1. A) Percentage of B(*a*)P sorbed to GO and to GO(PVP) for the three nominal incubation concentrations, and B) their corresponding sorption isotherms. C) Percentage of PAHs from WAF sorbed to GO for WAF dilutions tested, and D) their corresponding sorption isotherms. Lines represent isotherms fitted by the Linear (curved line) and Freundlich model (straight line).

The PAH concentration of the three WAF dilutions (6.25, 25 and 100%) of the NNS crude oil is shown in Table S4. The WAF produced from NNS oil presented low concentrations of the 18 PAHs analysed (ΣPAHs = 171.06 μg/L for 100% WAF). The compounds that could be measured in the three WAF dilutions were naphthalene, acenaphthene, fluorene and phenanthrene, with concentrations in the 100% sample of 163.245 μg/L, 0.951 μg/L, 3.779 μg/L and 2.874 μg/L, respectively. Thus, analyses of the sorption to GO were done for these four PAHs (Fig. 1C) that showed good recovery values (88.76–150.55%) after centrifugation of the control samples (Table S2). Phenanthrene was the PAH showing the highest sorption to GO with a 95.7% of sorption for 100% WAF, 99.2% for 25% WAF and 100% for 6.25% WAF. This was followed by fluorene with sorption values between 84.4 and 100%, while acenaphthene and naphthalene presented values of sorption to GO that ranged from 51.5 to 87.3% and from 9.7 to 21.3%, respectively. These results clearly indicated that the ability of PAHs to sorb to GO was dependent on their hydrophobicity.

Constants and parameters for WAF PAH sorption isotherm models are given in Table 1. Sorption isotherm models (Fig. 1D) were applied only for those PAHs detected in control samples (C_e > L.Q.) of the three WAF dilutions. According to the Linear sorption model, naphthalene and acenaphthene showed a nonlinear trend with a R^2 coefficient of 0.44 and 0.18, respectively. For the more hydrophobic PAHs, fluorene and phenanthrene, a linear trend was observed (R^2 of 0.85 and 0.92, respectively). K_d values were closely related to PAH hydrophobicity showing the following trend: phenanthrene > fluorene > acenaphthene > naphthalene. According to the Freundlich model, phenanthrene (R^2 = 0.87) and fluorene (R^2 = 0.89) fitted better than acenaphthene (R^2 = 0.34) and naphthalene (R^2 = 0.53), as also seen in the Linear model. In addition, values of sorption capacity (K_f) agreed with K_d values, with the exception of naphthalene and acenaphthene. Naphthalene showed higher K_f value than acenaphthene (19.71 versus 9.40 $(\mu g/g)/(L/\mu g)^N$), but lower K_d value (1.55 versus 4.56 L/g). Cooperation between the PAHs and GO (N) was higher for naphthalene (N = 0.60) and phenanthrene (N = 0.65) than for fluorene (N = 0.49) or acenaphthene (N = 0.34).

3.2. Characterisation of GO NMs

Micrographs of the three GO NMs obtained by TEM and AFM are shown in Fig. S2. At TEM, platelets with different sizes and shapes were observed, being the maximum length of the platelets always below 13 μm. According to AFM analysis, thickness of GO platelets was 0.612 ± 0.176 nm (n = 3), in agreement with the information provided by the provider. An increase of thickness was observed for GO(PVP) platelets with a value of 1.994 ± 0.319 nm (n = 3). rGO(PVP) platelets appeared thicker than GO and GO(PVP) platelets, with a value of 4.174 ± 0.179 nm. Platelets of GO-B(*a*)P and GO(PVP)-B(*a*)P showed similar length to GO or GO(PVP) alone (Fig. S3). GO-B(*a*)P presented a thickness of 0.796 ± 0.177 nm (n = 3) and GO(PVP)-B(*a*)P presented a thickness of 3.995 ± 0.221 nm (n = 3). No relevant aggregation of GO platelets was observed with or without B(*a*)P, but an increase of thickness was observed in GO(PVP)-B(*a*)P platelets compared to GO (PVP) alone.

Table 1
Estimated parameters for the Linear and the Freundlich models explaining the sorption of B(*a*)P to GO and to GO(PVP), and the sorption of PAHs from a naphthenic North Sea oil WAF to GO.

		Linear model		Freundlich model			n
		K_d	R^2	K_f	N	R^2	
GO	Benzo(*a*)pyrene	756.58	0.88	665.47	1.59	0.83	9
GO(PVP)	Benzo(*a*)pyrene	575.05	0.91	357.78	1.52	0.89	9
GO	Naphthalene	1.55	0.44	19.71	0.60	0.53	7
	Acenaphthene	4.56	0.18	9.40	0.34	0.34	9
	Fluorene	46.92	0.85	73.85	0.49	0.89	9
	Phenanthrene	307.27	0.92	188.87	0.65	0.87	9

K_d = partition coefficient of PAHs between GO and the aqueous phase at equilibrium (L/g); K_f = Freundlich affinity coefficient $[(\mu g/g)/(L/\mu g)^N]$; N = site energy heterogeneity factor; n = number of samples.

3.3. Embryo toxicity tests and localisation of fluorescent rGO in zebrafish embryos

The results of the developmental parameters of zebrafish embryos exposed to GO NMs alone or in combination with PAHs are shown in Table 2 and the odd ratio values for each treatment showing statistically significant differences and their corresponding confidence intervals are shown in Table S5. Survival at 120 hpf and hatching time did not show statistically significant differences between treated and control embryos, neither for GO alone nor in combination with PAHs. Regarding malformation prevalence at 120 hpf, unexposed control embryos showed values ranging from 0 to 11.4%. Exposure to 5 and 10 mg/L of GO caused a significant increase in total malformation prevalence, reaching to 33.3% and 23.3%, respectively. Exposure to 10 mg/L of rGO(PVP) also caused significantly higher malformation prevalence (26.7%) than in control embryos. Embryos exposed to GO(PVP) did not show any significant difference on malformation prevalence for the exposure concentrations used. Looking at malformation prevalences produced by the GO NMs in combination with PAHs, GO(PVP)-B(*a*)P was the most toxic combination to zebrafish embryos. Embryos exposed to 0.5, 5 and 10 mg/L of GO(PVP)-B(*a*)P presented a significant increase (20%, 13.8% and 26.7%, respectively) compared to unexposed embryos. In the case of GO-B(*a*)P, only embryos exposed to 5 mg/L showed a malformation prevalence (28.6%) higher than controls. None of the GO + WAF concentrations used caused significant toxicity to embryos in terms of increased malformation prevalence. At the same exposure concentration, no significant differences were found between embryos exposed to GO NMs alone or with sorbed PAHs.

The most prevalent malformation among exposed embryos was spinal cord flexure (Fig. S4B). This malformation was mostly observed in embryos exposed to 5 mg/L of GO and GO(PVP) with a malformation prevalence of 25.9% and 26.7%, respectively. The highest prevalence of pericardial edema was observed in embryos exposed to 10 mg/L of rGO(PVP) (Fig. S4C) with a 20% of prevalence and in embryos exposed to 5 mg/L of GO-B(*a*)P with a prevalence of 17.9% (Fig. S4D). Embryos exposed to 10 mg/L of GO(PVP)-B(*a*)P also showed a high prevalence of pericardial edema (16.7%). Embryos showing yolk sac edema and eye abnormality were found among those exposed to GO (Fig. S4E), GO(PVP) (Fig. S4F) and GO + WAF (Table 2).

Values of EC_{50} and EC_{10} for malformation occurrence calculated for all the treatments are shown in Table S6. GO + WAF was the most toxic treatment for embryos according to the EC_{10} value (0.39 ± 2.11 mg/L). EC_{10} values were similar for embryos exposed to rGO (PVP), GO(PVP)-B(*a*)P and GO-B(*a*)P (3.03 ± 1.37 mg/L, 3.14 ± 1.43 mg/L and 4.08 ± 1.99 mg/L, respectively). These values could not be calculated for GO and GO(PVP). EC_{50} values for all the treatments were higher than the highest exposure concentration (10 mg/L). The lowest EC_{50} values corresponded to GO (14.67 ± 4.03 mg/L) and to rGO(PVP) (14.52 ± 3.12 mg/L). Similar values were estimated for zebrafish embryos exposed to GO + WAF (16.07 ± 4.98 mg/L) and GO(PVP)-B(*a*)P (15.11 ± 3.51 mg/L). The highest EC_{50} values among treatments for zebrafish embryos were recorded for GO-B(*a*)P (20.57 ± 8.03 mg/L) and GO(PVP) (30.98 ± 26.7 mg/L).

Zebrafish embryos were exposed for 120 h to Fl-rGO in order to track rGO fate in the embryos. At 120 hpf, unexposed embryos did not show fluorescence (Fig. S5A–B) whereas fluorescence was observed in the yolk sac and digestive tract of zebrafish embryos exposed to 1 (Fig. S5C–D) and 10 mg/L (Fig. S5E–F) of Fl-rGO.

Table 2
Results of the developmental parameters (% of surviving embryos at 120 h, hatching time and % of malformed embryos at 120 h) of zebrafish embryos exposed to graphene NMs alone and in combination with PAHs. Asterisks indicate statistically significant differences ($p < 0.05$) compared to the control group according to the binomial logistic regression. The values of the corresponding odd ratios are given in Table S4. Values for hatching time are given as means ± S.D.

	Concentration (mg/L)	Survival (%)	Hatching time (h)	Malaformation (%)	Type of Malaformation (%)			
					SC	PE	YE	EA
GO	0	100	72	8.3	8.3	8.3	0	0
	0.1	100	72	20	20	20	0	0
	0.5	90	70.4 ± 6.41	13.8	13.8	3.5	3.5	3.5
	1	100	72	3.3	3.3	0	0	0
	5	96.7	71.2 ± 4.46	33.3*	25.9	7.4	7.4	7.4
	10	100	72.0	23.3*	23.3	0	0	0
GO(PVP)	0	97.2	66.91 ± 9.74	11.4	11.4	0	0	0
	0.1	96.7	70.22 ± 8.42	16.7	16.7	0	0	0
	0.5	100	68 ± 10.32	24.1	13.8	10.3	6.9	6.9
	1	100	67.2 ± 9.76	20	16.7	3.3	0	0
	5	96.7	66.4 ± 9.23	30	26.7	3.3	0	0
	10	100	68.8 ± 6.09	20.7	13.8	6.9	0	0
rGO(PVP)	0	100	68.67 ± 8.42	5.6	2.8	2.8	0	0
	0.1	100	68 ± 4.38	3.3	3.3	0	0	0
	0.5	100	66.4 ± 4.38	6.7	0	6.7	0	0
	1	100	66.4 ± 10.32	6.7	6.7	0	0	0
	5	100	71.2 ± 10.32	20	16.7	3.3	0	0
	10	100	71.2 ± 9.10	26.7*	10	20	0	0
GO + WAF	0	94.4	70.55 ± 5.73	2.9	2.9	0	0	0
	0.1	96.7	69.42 ± 7.82	3.8	3.8	0	0	0
	0.5	86.7	70 ± 4.71	19.2	15.4	3.8	0	0
	1	93.3	70.31 ± 6.29	10.7	7.1	3.6	0	0
	5	86.7	71.2 ± 6.52	23.1	23.1	0	0	0
	10	86.7	69.33 ± 7.4	25.1	25.1	3.4	3.4	3.4
GO-B(*a*)P	0	97.2	72	5.7	5.7	0	0	0
	0.1	100	71.2 ± 4.38	3.7	0	3.7	0	0
	0.5	93.3	71.2 ± 4.54	0	0	0	0	0
	1	93.3	72	3.6	3.6	0	0	0
	5	90	70.86 ± 4.62	28.6*	10.7	17.9	0	0
	10	90	71 ± 4.62	10	3.3	6.7	0	0
GO(PVP)-B(*a*)P	0	100	72	0	0	0	0	0
	0.1	100	72	0	0	0	0	0
	0.5	96.7	72	20*	20	0	0	0
	1	96.7	72	6.9	3.4	3.4	0	0
	5	100	72	13.8*	10.3	6.9	0	0
	10	96.7	72	26.7*	13.4	16.7	0	0

SC = spinal cord flexure; PE = pericardial edema; YE = yolk sac edema; EA: eye abnormality.

3.4. Accumulation and effects in adult zebrafish

3.4.1. GO and PAH concentrations in water and PAH bioaccumulation in adult fish

Up to 24 h after dosing, measured GO concentrations in exposure tanks containing GO (GO, GO + WAF and GO-B(*a*)P) were close to the nominal GO concentration (2 mg/L) in the two assessed cycles (3rd and 7th, Fig. S6). Then, GO concentration decreased close to the limit of detection (0.5 mg/L) at 72 h, except in the case of GO-B(*a*)P and GO + WAF tanks during the third dose, where an unexpected GO concentration increase was measured.

Summarised results of PAH concentrations over time for each tank during the first three days of exposure of adult zebrafish are shown in Table S7. Control tank presented low concentrations of the analysed PAHs, below or near the limit of quantification, and with similar values along time. Total PAH concentration in GO + WAF tank decreased 130 times from 5 min (8044.1 ng/L) to 72 h after adding the contaminants (61.1 ng/L). Naphthalene was the most abundant PAH in the water samples with a decrease of concentration from 7788.9 ± 491.9 ng/L at 5 min to 4730.9 ± 122.1 ng/L at 8 h after dosing. Naphthalene concentration reached 34.9 ± 3.4 ng/L after 72 h. The concentration of the other measured PAHs, acenaphthene, fluorene, phenanthrene and anthracene also decreased progressively along time almost reaching limits of quantification after 72 h of dosing. B(*a*)P was not detected in this treatment. B(*a*)P concentration in the GO-B(*a*)P exposure tank was more stable than in the previous case with an initial concentration of 1743.2 ± 117.3 ng/L and a concentration at 72 h of 1293.2 ± 309.2 ng/L. In the case of exposure to B(*a*)P alone, measured concentration at 5 min was 29,440.3 ± 4582.1 ng/L, remained stable up to 8 h (34,682.5 ± 4147 ng/L) and decreased progressively up to 7956.7 ± 1723.1 ng/L at 72 h.

PAH accumulation in whole zebrafish after 21 days of exposure is shown in Table 3. While control fish presented a total PAH value of 44.82 ± 10.20 ng/g, fish exposed to GO + WAF presented a total PAH concentration of 139.16 ± 24.79 ng/g, being fluorene and phenanthrene the most accumulated compounds. B(*a*)P was not detected in these treatments. Fish exposed to GO-B(*a*)P accumulated B(*a*)P up to a concentration of 37.49 ± 11.28 ng/g, while B(*a*)P concentration in fish exposed only to B(*a*)P reached 10,065.38 ± 1444.03 ng/g.

3.4.2. Localisation of GO in adult zebrafish

Rod-like structures resembling longitudinal sections of GO platelets were detected at histological level in the lumen of the intestine of the zebrafish exposed to all treatments that contained GO (GO, GO + WAF, GO-B(*a*)P) at the two exposure times (Fig. 2). Unexposed embryos did not show the presence of these putative GO platelets. TEM analysis also showed the presence of GO platelets in the lumen of the intestine of zebrafish (Fig. 2). The length of the GO platelets found in the intestine ranged from 0.9 to 2.7 μm which

Table 3
Concentration of PAHs (ng/g) in adult zebrafish at 21 days of exposure. Values are represented as mean ± S.D.

	Control	GO + WAF	GO-B(*a*)P	B(*a*)P	L.Q.
Naphthalene	<L.Q.	<L.Q.	–	–	9.0
Acenaphthylene	1.07 ± 0.12	2.60 ± 0.63	–	–	0.6
Acenaphthene	4.69 ± 0.42	18.21 ± 3.68	–	–	2.0
Fluorene	9.48 ± 0.62	56.57 ± 9.91	–	–	1.0
Phenanthrene	18.30 ± 5.84	44.84 ± 6.92	–	–	10.0
Anthracene	0.94 ± 0.83	4.72 ± 0.70	–	–	0.5
Fluoranthene	4.61 ± 1.53	4.13 ± 1.01	–	–	3.0
Pyrene	5.74 ± 0.84	8.08 ± 1.95	–	–	4.0
Benzo(*a*)pyrene	<L.Q.	<L.Q.	37.49 ± 11.28	10,065.38 ± 1444.03	1.0
ΣPAHs	44.82 ± 10.20	139.16 ± 24.79			

L.Q.: limit of quantification; −: not measured.

agreed well with the data of isolated GO platelets analysed by AFM and TEM (<10 μm). GO was not seen inside the cells, neither at light microscopy nor at TEM level.

3.4.3. Transcription levels of target genes

The transcription levels of selected genes are represented in Fig. 3. For genes related with biotransformation metabolism, only *cyp1a* transcription levels showed significant differences between fish exposed to GO and those exposed to B(*a*)P at 3 days. In the case of transcription levels of *tp53*, only fish exposed to GO-B(*a*)P showed a significantly higher transcription level than fish exposed to GO + WAF at 3 days. Regarding the transcription level of genes related with oxidative stress, no significant differences were found among groups at 3 or 21 days of exposure (Fig. 3).

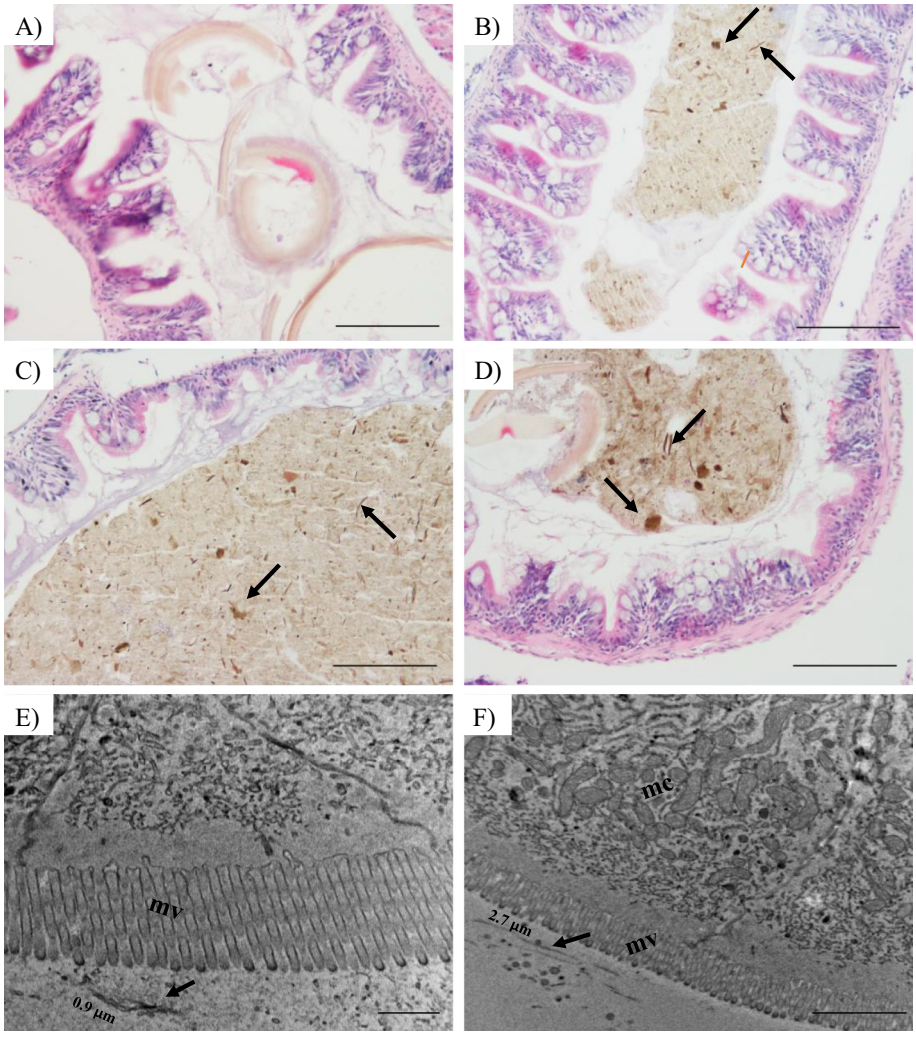

Fig. 2. Localisation of GO in adult zebrafish intestine. Micrographs of histological sections of A) unexposed adult zebrafish at 21 days showing normal intestine histology and remnants of brine shrimp capsules in the lumen; B) adult zebrafish exposed to 2 mg/L of GO for 21 days; C) adult zebrafish exposed to 2 mg/L of GO + WAF for 21 days; D) adult zebrafish exposed to 2 mg/L of GO-B(*a*)P for 21 days. Fish exposed to treatments containing GO showed abundant putative GO platelets in the lumen of the intestine (arrows). E–F) TEM micrographs showing the apical zone of the enterocytes of adult zebrafish after 21 days of exposure to 2 mg/L GO. The presence of GO platelets (arrows) was detected in the digestive lumen, but not inside enterocytes. Microvilli (mv), mitochondria (mc). Scale bars: A–D) 100 μm, E) 0.5 μm and F) 2 μm.

3.4.4. Biochemical biomarkers

Results of the biotransformation metabolism and oxidative stress biochemical biomarkers in liver and gills of adult zebrafish are shown in Fig. 4. All treated groups showed higher EROD activity in liver than controls fish at 3 days, being significantly higher in B(*a*)P-exposed fish. After 21 days of exposure, significant differences among groups were not observed, although fish exposed to B(*a*)P maintained the highest EROD activity (Fig. 4A). EROD activity in gills did not show any significant differences, neither among experimental groups nor between exposure times (Fig. 4B).

After 3 days of exposure, GST activity in liver did not show any significant differences compared to control fish. After 21 days, fish exposed to B(*a*)P alone showed significantly higher activity than fish exposed to GO-B(*a*)P, but no differences were detected respect to control fish. A significant increase of activity at 21 days compared to 3 days was recorded for control fish, and in fish exposed to GO + WAF and to B(*a*)P (Fig. 4C). In gills, GST activity was significantly higher in fish exposed to GO + WAF than in fish exposed GO for 3 days (Fig. 4D). After 21 days, GST activity in gills of fish exposed to GO + WAF decreased compared to fish sampled after 3 days of exposure. Also at 21 days, fish exposed to GO-B(*a*)P presented significantly higher activity than fish exposed to GO. Catalase activity did not change significantly in zebrafish liver among exposure groups or between exposure times (Fig. 4E). In gills, at 3 days, catalase activity was higher in all exposed groups than in control fish, being significantly higher for fish exposed to GO-B(*a*)P and B(*a*)P (Fig. 4F). After 21 days, CAT activity remained higher in treated fish than in control fish, but only in fish exposed to GO-WAF it was significantly higher than in control fish.

Regarding AChE activity in brain, no significant differences were detected at 3 days of exposure (Fig. 4G). At 21 days, AChE was significantly lower in the brain of all exposed fish than in the brain of control fish, suggesting signs of neurotoxicity. A significant increase of activity was recorded in control fish at 21 days compared to 3 days while a significant decrease was measured in GO + WAF exposed fishes.

3.4.5. Histopathological alterations

Results of the histopathological evaluation of liver tissue is shown in Table S8. Control fish showed, in general, normal architecture of the liver (Fig. 5A). An overall increase in the prevalence of liver vacuolisation was recorded in all treated groups, being significant compared to the control group in fish exposed to GO + WAF for 3 days (60%) and 21 days (50%) (Table S8). Megalocytosis was found in two individuals, one exposed to GO + WAF and another treated with B(*a*)P (Fig. 5C). Other histopathological alterations that are commonly found in liver, such as necrotic foci or eosinophilic foci were not observed in the liver of any treated or control individual. In gill tissues, not significant differences in the prevalences of histopathological conditions were observed, as shown in Table S9. Control fish showed in general normal architecture of the gills (Fig. 5E). Some of the histopathological lesions found in gills were inflammation and aneurism of the secondary lamella, being the highest prevalence of aneurism observed in fish exposed to B(*a*)P (33.3%) and to GO-B(*a*)P (20%) for 21 days (Fig. 5H). Only one individual presented hyperplasia of the primary lamellae.

4. Discussion

To assess the potential risk of graphene NMs as vectors of PAHs, the capacity of the NMs to sorb these organic compounds needs to be analysed. In the present work, we selected for this analysis B(*a*)P, as a model pyrolytic PAH, and the WAF of a crude oil, as an environmentally relevant mixture of petrogenic PAHs. B(*a*)P recovery in the control samples after centrifugation needed to separate GO platelets from the liquid phase was lower than expected, due to its high hydrophobicity. In addition, measured B(*a*)P concentration in water differed from the nominal

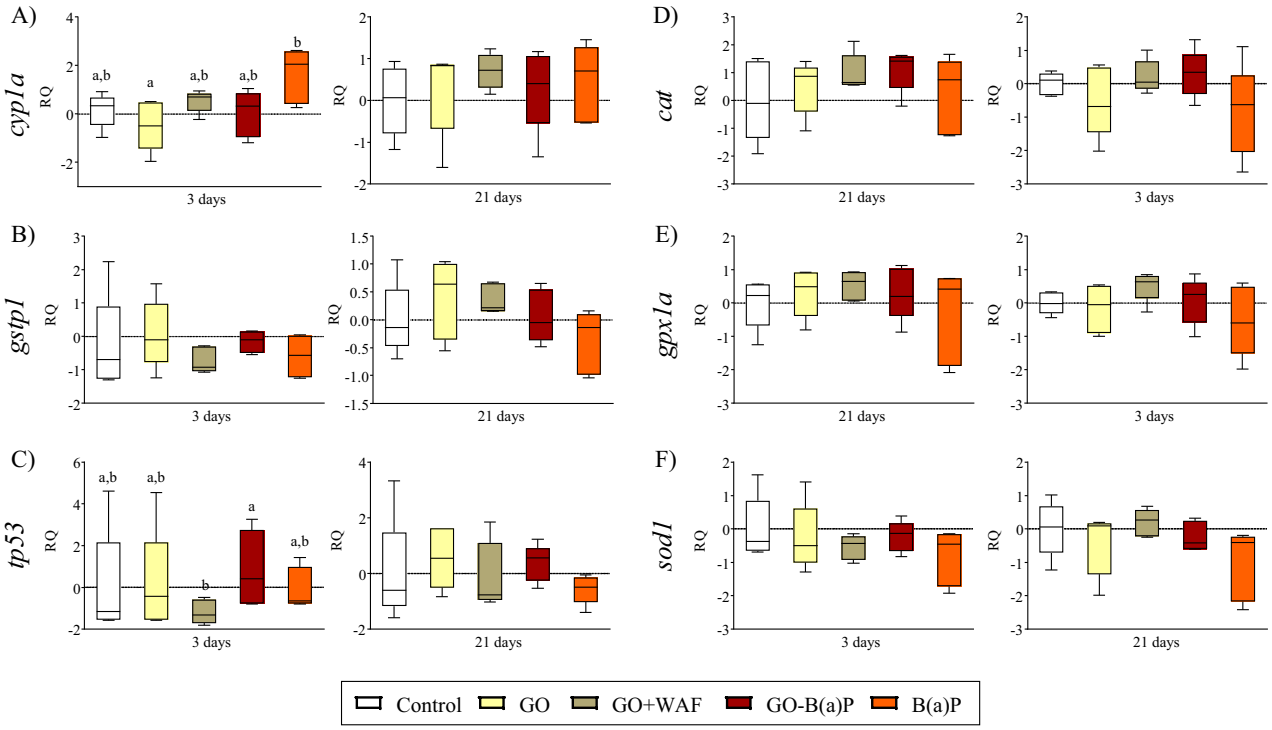

Fig. 3. Relative quantification (RQ) of transcription levels of the biotransformation metabolism related genes A) *cyp1a* and B) *gstp1*, C) tumour suppressor gene *tp53* and oxidative stress related genes D) *cat*, E) *gpx1a* and F) *sod1* in adult zebrafish liver after 3 and 21 days of exposure to GO, GO + WAF, GO-B(*a*)P and B(*a*)P. Box-plot boxes represent the percentage data values in between the 25th and the 75th percentile, median indicated by a line in the middle of the box. Whiskers are the data values in up to the 5th percentile and 95th percentile. Different letters indicate statistically significant differences ($p < 0.05$) within each sampling time according to the Kruskal-Wallis test followed by C, E) the post hoc Dunn's test for non-parametric data and to A, B, D, F) one-way ANOVA followed by the post hoc Tukey's test.

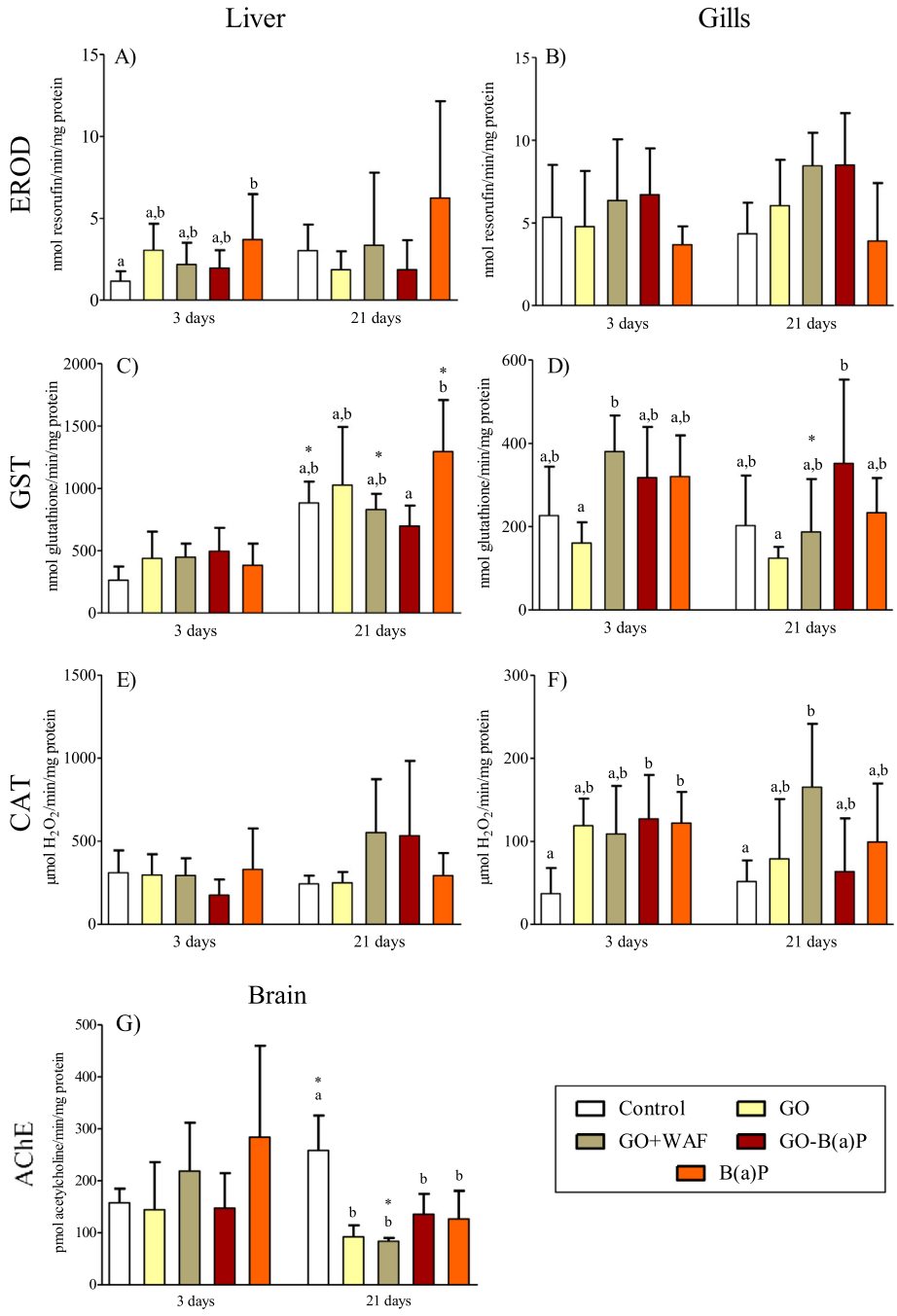

Fig. 4. Results of the biochemical biomarkers measured in adult zebrafish after 3 and 21 days of exposure to GO, GO + WAF, GO-B(*a*)P and B(*a*)P. A) EROD activity in liver and B) gills, C) GST activity in liver and D) gills, E) CAT activity in liver and F) gills and G) AChE activity in brain. Different letters indicate statistically significant differences ($p < 0.05$) within each sampling time according to A, B, C, E, G) the Kruskal-Wallis test followed by the post hoc Dunn's test for non-parametric data and D, F) one-way ANOVA followed by the post hoc Tukey's test for parametric data. Asterisks indicate statistically significant differences ($p < 0.05$) for the same treatment between exposure days according to the Mann-Whitney's *U* test for non-parametric data and Student's *t*-test for parametric data.

concentration (sorption experiments, adult exposure group). B(*a*)P use above saturation point (B(*a*)P water solubility, 1.62 µg/L; ChemIDplus, 2020) usually leads to lower concentration in water than expected (Zhao et al., 2013). Working with over saturated B(*a*)P concentration was needed to achieve high levels of PAH sorption to GO that could further produce toxic effects in aquatic organisms. According to the results, GO showed a great ability to sorb B(*a*)P; between 87.2% and 100% of the total B(*a*)P in the incubation media was sorbed to GO. B(*a*)P also showed the highest K_f value (665.47 (µg/g)/(µg/L)^N) and a Freundlich N factor of 1.59. In the case of the complex mixture formed in the WAF of the NNS crude oil, the sorption of PAHs to GO was mainly explained by their hydrophobicity. According to the K_f values of the Freundlich isotherm model, sorption of PAHs to GO was as follows: acenaphthene < naphthalene < fluorene < phenanthrene. The highest K_f value was obtained for phenanthrene (188.87 (µg/g)/(µg/L)^N) with a Freundlich N factor of 0.65. Those values were lower than those obtained for B(*a*)P, as expected based on their lower hydrophobicity and number of aromatic rings. To the best of our knowledge, no previous works have experimentally studied the sorption of B(*a*)P to GO, but Li et al. (2018) published some predictive simulations that agree with our results. Regarding other PAHs, Wang et al. (2014) evaluated the sorption capacity of naphthalene, phenanthrene and pyrene to

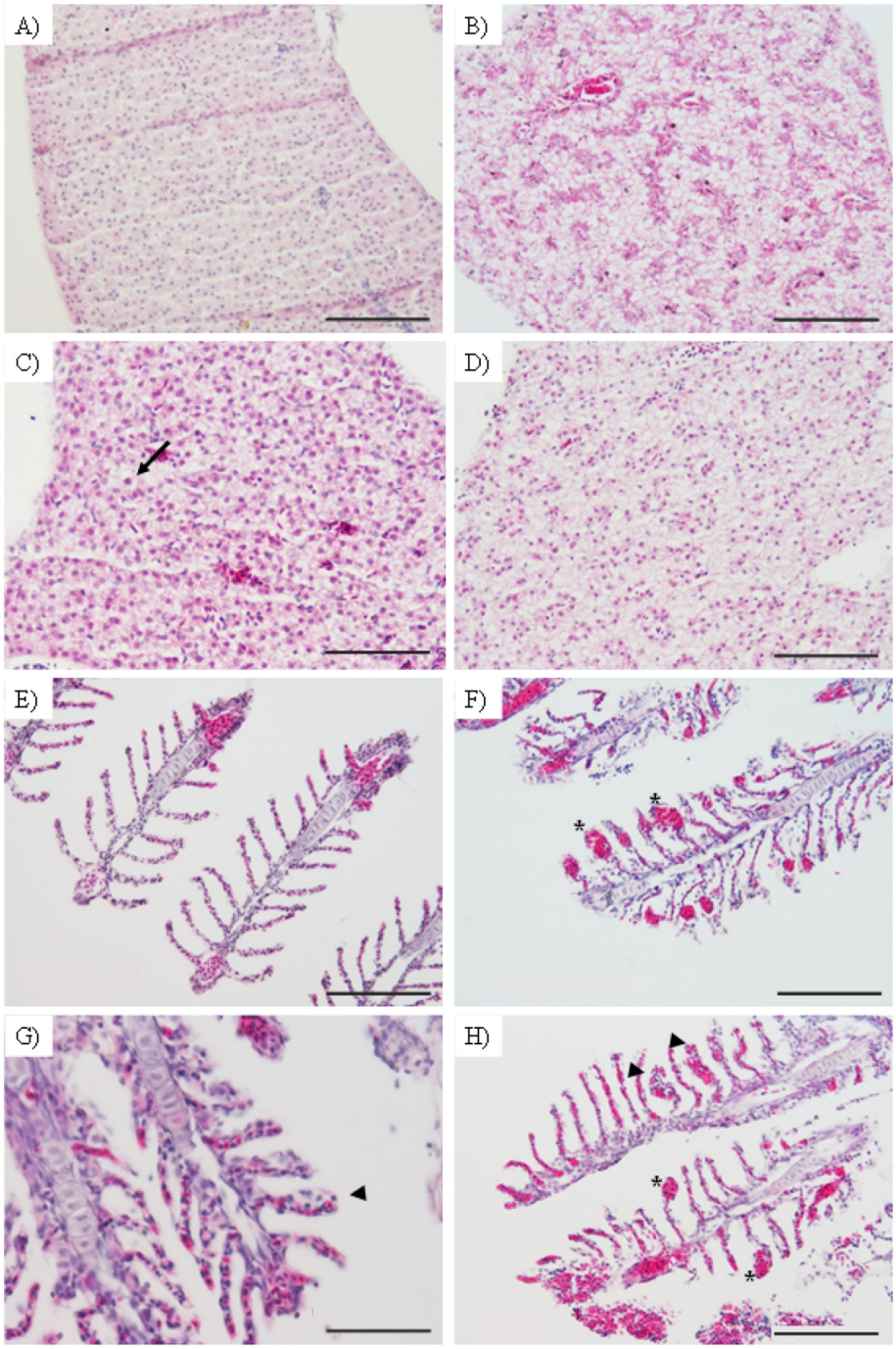

Fig. 5. Micrographs of histological sections of zebrafish liver and gills. A) Liver of unexposed adult zebrafish at 21 days showing normal morphology; B) Liver of zebrafish exposed to GO for 3 days showing liver vacuolisation; C) Liver of a zebrafish exposed to GO + WAF for 21 days showing megalocytosis (black arrow); D) Liver of a zebrafish exposed to GO-B(*a*)P for 21 days showing liver vacuolisation; E) Gills of unexposed adult zebrafish at 3 days showing normal morphology; F) Gills of zebrafish exposed to GO for 3 days, showing aneurisms (asterisks) of the secondary lamellae; G) Gills of a zebrafish exposed to GO + WAF for 3 days, showing inflammation (arrow head); H) Gills of a zebrafish exposed to GO-B(*a*)P for 3 days, showing inflammation (arrow head) and aneurisms (asterisks) of the secondary lamellae. Scale bars: A–D) 100 μm, G) 50 μm and E, F, H) 25 μm.

graphene and to GO. Values of K_f for GO increased with the increase in the number of aromatic rings and hydrophobicity of each PAH, with values of 0.776 ± 0.0328 $(mg/g)/(L/mg)^N$, 8.12 ± 0.257 $(mg/g)/(L/mg)^N$ and 42.3 ± 5.39 $(mg/g)/(L/mg)^N$, respectively. This tendency was also observed in the present study, with the exception of the higher K_f value (19.71 $(\mu g/g)/(L/\mu g)^N$) and N factor (0.60) obtained for the sorption of naphthalene to GO compared to those reported in the literature (Pei et al., 2013; Wang and Chen, 2015) and even higher than the values obtained for acenaphthene (a PAH heavier than naphthalene) in the present study. The WAF produced from NNS oil presented low concentrations of the 18 PAHs analysed (ΣPAHs = 171,059.5 ng/L for 100% WAF), partially due to the low energy (no vortex) used for its production, as it has been reported for other crude oils. In the case of the Deepwater Horizon oil, PAH concentration increased from 4 to 196 μg/L in WAFs produced at low energy to 263–6006 μg/L in WAFs produced at higher energy (Forth et al., 2017). In the present study, naphthalene was the most abundant PAH in the WAF (163,244.5 ± 1961.3 ng/L), representing 95% of the total PAH concentration. Competition among

PAHs for sorption onto GO surface could explain the K_f and N factor values estimated. Low values of the Freundlich fitted "N" factor indicate an inhomogeneous distribution of PAHs onto GO surface with a wide adsorption site distribution of the PAHs (Carter et al., 1995). The competition between PAHs on GO platelets was higher for phenanthrene and naphthalene being distributed more homogenously and less widely than the other PAHs. In accordance, a higher K_f coefficient was obtained for naphthalene than for acenaphthene, but values for phenanthrene and fluorene were still higher than for naphthalene. Only one work that studied the potential sorption of a complex PAH mixture to rGO was found in the literature (Sun et al., 2013). In this case, sorption of the PAHs to rGO was mainly driven by the initial concentration and not by the PAH characteristics (Sun et al., 2013). Naphthalene, as the most concentrated PAH in the WAF, was expected to cover the surface of GO at a higher extent than the other PAHs. Nevertheless, initial concentration is not the only parameter regulating the sorption process to GO; the main parameter, as previously mentioned, was hydrophobicity.

GO showed a high capacity to sorb B(*a*)P, without major differences in the presence of PVP. Nevertheless, when applying isotherm sorption models, values of K_d and K_f were higher for GO (756.58 L/g and 665.45 $(\mu g/g)/(L/mg)^N$) than for GO(PVP) (575.05 L/g and 357.55 $(\mu g/g)/(L/\mu g)^N$). The use of PVP (polymer-surfactant) that interacts with GO through hydrogen bonds, allows to disperse GO in the suspension by changing its surface characteristics and making GO platelets completely compatible with water (Zhang et al., 2010). The lower hydrophobicity of the GO(PVP) platelets due to the presence of the surfactant makes GO less likely for hydrophobic compounds sorption than GO alone.

Addition of PVP and reduction of GO resulted into thicker GO(PVP) and rGO(PVP) platelets than GO platelets, as previously reported in the literature (Luque-Alled et al., 2020; Zhang et al., 2010); this increase is suggested to be caused by PVP nanospheres that make the platelets thicker. The GO centrifugation process after contamination with B(*a*)P did not alter the lateral dimensions or the thickness of the platelets and no evidence of stacking was observed. In the case of GO(PVP) platelets, an increase of thickness was observed after contamination with B(*a*)P, which suggested that the proven sorption of B(*a*)P to GO(PVP) and the previously reported PVP effect on thickness could change the surface charge producing the stacking and aggregation of the platelets.

Given the capacity of GO to sorb PAHs, GO contaminated with B(*a*)P and with PAHs from WAF was assessed for potential toxicity on zebrafish development. Survival and hatching time of zebrafish embryos were not significantly altered by any treatment or concentration used. A significant increase of malformation prevalence was observed only for the highest concentrations assayed and for 0.5 mg/L of GO (PVP)-B(*a*)P, although all EC_{50} values were higher than the highest concentration tested (10 mg/L). Based on calculated EC_{50} values for malformation occurrence, the following toxicity ranking was observed: rGO (PVP) > GO > GO(PVP)-B(*a*)P > GO + WAF > GO-B(*a*)P > GO(PVP). As reported in the literature, zebrafish embryos exposed to GO (0.01–100 mg/L) presented malformations, such as yolk sac edema and spinal cord flexure, for GO concentrations ranging from 1 to 5 to 100 mg/L (Chen et al., 2016a; D'Amora et al., 2017). In addition, changes in hatching rate of zebrafish embryos exposed from 50 to 100 mg/L of GO have been reported (D'Amora et al., 2017). Z. Yang et al. (2019) observed similar malformations in embryos exposed to 1 and 10 mg/L of GO, which showed upregulation of immune response related genes and signs of oxidative stress (increased superoxide dismutase and catalase activities and glutathione concentration) compared to control embryos for the highest GO concentration. Some sublethal effects (oxidative stress and neurotoxicity) are reported in the literature in zebrafish embryos after exposure to lower GO concentrations (1–100 μg/L) than those used in the present work. Acute effects (malformation prevalence and hatching delay) were only observed in zebrafish embryos for concentrations higher than 10 mg/L. Regarding different types of GO NMs, exposure of 5 and 50 mg/L of rGO, but not of GO, provoked changes in hatching rate and body length of zebrafish embryos, although no significant effects on zebrafish malformation and mortality were observed at the tested concentrations (Liu et al., 2014). Thus, evidences point that rGO is more toxic than GO as observed in our results in zebrafish embryos and in the literature, mainly due to the higher bioavailability of rGO (Katsumiti et al., 2017; Yan et al., 2017).

As to the best of our knowledge, modulation of PAH toxicity to zebrafish embryos in presence of GO has not been reported in the literature yet. Nevertheless, toxicity of another persistent pollutant, such as bisphenol A, in combination with GO was assessed by J. Yang et al. (2019). The availability of bisphenol A to zebrafish embryos was reduced in the presence of GO and adverse effects caused by bisphenol A on zebrafish embryos (larvae malformation and hatching delay) were alleviated. Similar findings have been published for other non-planar carbon NMs, such as fullerenes (C_{60}) and carbon nanotubes, in combination with PAHs (Della Torre et al., 2018; Falconer et al., 2015). The accumulation of B(*a*)P (1 mg/L) was reduced in presence of C_{60} (20 mg/L), but similar toxicity was observed for C_{60} alone or in combination with B(*a*)P (Della Torre et al., 2018). Phenanthrene (10 mg/L) was also less available to zebrafish embryos in presence of multiwalled carbon nanotubes (50–200 mg/L MWCNTs) (Falconer et al., 2015). An increase of MWCNTs concentration to 200 mg/L, with the same phenanthrene concentration, increased the survival rate of zebrafish embryos compared to embryos exposed to phenanthrene alone. Presence of GO might reduce the availability of PAHs decreasing their toxicity at the tested concentrations, and it can be suggested that the toxicity observed on zebrafish embryo development was mainly due to the GO characteristics rather than to PAH toxicity.

The effects produced by GO on zebrafish embryos could be due to the ingestion-internalisation of GO (Chen et al., 2015; J.H. Zhang et al., 2017). Thus, GO labelled with fluorescein was observed inside zebrafish embryos at early development (24 hpf), indicating the ability of GO to cross the chorion barrier. Fluorescence produced by GO was more intense in the chest than in the head or in the tail. A similar accumulation patter was observed for fluorescent rGO on zebrafish embryos (Chen et al., 2015). rGO internalisation was already observed at 12 hpf in exposed embryos, while GO was first internalised in zebrafish embryos at 24 hpf (J.H. Zhang et al., 2017).

To further understand the effects of GO alone or in combination with PAHs, an experiment with adult zebrafish was carried out. The selected GO concentration (2 mg/L) has been used in previous studies (Souza et al., 2017) and showed effects in adult zebrafish, while being a relatively low concentration. GO is stable at long term in freshwater (Chowdhury et al., 2013), but the presence of fish and, consequently, of organic matter due to fish feeding could produce GO aggregation in the exposure tanks (Souza et al., 2017; Castro et al., 2018), which could lead to an heterogeneous dispersion of GO in the tanks and could explain the variability in GO concentrations measured in water, especially during the first three days of the experiment. Nevertheless, the system appeared to stabilise and in the last three days of exposure, the concentration of GO in the three GO-containing tanks behaved similarly. Changes in GO concentration in water could also be due to the ingestion of GO by zebrafish as proved in the present study. The ingestion of GO by aquatic organisms has been shown by TEM analysis (Hu et al., 2017). GO translocation from water to adult zebrafish brain was reported by Hu et al. (2017). Also, GO was found in the diencephalon of the offspring of the adult zebrafish exposed to 1 μg/L of GO, demonstrating that GO can be transferred from the adult to the offspring through gametes. In our study GO was identified in the lumen of the intestine of adult zebrafish but evidences of GO translocation to the tissues were not found.

Along with the quantification of the GO concentration in the exposure tanks, PAH levels were also measured. PAH concentration in the control tank was close to the limit of quantification. In the co-exposure GO + WAF tank, total PAH concentration was progressively reduced along the 72 h of the dosing cycle, mainly due to the reduction in naphthalene concentration. As previously discussed, naphthalene

was only partially sorbed to GO. Thus, the loss of naphthalene concentration could be expected due to its low hydrophobicity and high volatility (Salazar-Coria et al., 2019). A similar decrease of PAH concentration over time was measured in the B(*a*)P alone exposure tank, where B(*a*)P concentration was reduced from 29,440.3 ± 4582.1 ng/L to 7956.7 ± 1723.1 ng/L over 72 h, a reduction that could be partially explained by the high capacity of fish to uptake and metabolise PAHs (Livingstone, 1998). Overall, PAH exposure levels were not constant over time, except in the case of GO-B(*a*)P exposure group, where B(*a*)P concentration remained almost stable for 72 h (1743.2 ng/L to 1293.2 ng/L), possibly as a consequence of desorption of B(*a*)P from GO.

PAH bioaccumulation was also analysed in zebrafish in order to confirm fish exposure. Except for naphthalene, PAH accumulation in zebrafish exposed to GO + WAF reflected the PAH concentration in exposure media. Despite of the high concentration of naphthalene in the GO + WAF exposure tank, accumulation of this compound in zebrafish was not detected in this study. The bioavailability of PAHs sorbed to carbon NMs was studied by Linard et al. (2017) who concluded that bioavailability to freshwater fish of PAHs associated with graphene was higher for the most hydrophobic PAH phenanthrene (90% of adsorbed phenanthrene was bioavailable), than for anthracene, fluorene or naphthalene (35%, 40% and 20%, respectively). A lower PAH bioaccumulation was measured in fish exposed to GO-B(*a*)P than in those co-exposed to GO + WAF in agreement with PAH concentration in exposure media. Another factor to be considered regarding PAH bioaccumulation is the capacity of the fish to metabolise those compounds, being more hydrophobic PAHs more easily metabolised and excreted than lower weight PAHs being, in turn, less accumulated in fish (Livingstone, 1998). In addition, a noticeable accumulation of B(*a*)P in the whole body of fish exposed for 21 days to B(*a*)P alone was recorded, while fish exposed to GO-B(*a*)P showed much lower levels of B(*a*)P in their tissues as could be expected based on B(*a*)P levels measured in water. These results indicated that B(*a*)P sorbed to GO was less bioavailable than dissolved B(*a*)P, as previously discussed.

Analyses of the biological responses in adult zebrafish showed that fish exposed to B(*a*)P alone for 3 days presented the highest transcription levels of hepatic *cyp1a*. This up-regulation of *cyp1a* could have been translated into a significant induction of EROD activity in the liver of fish exposed to B(*a*)P for 3 days, that remained the highest among treatments after 21 days of exposure. This response is linked to the previously mentioned bioaccumulation of B(*a*)P in fish tissue at 21 days of exposure, although elimination (biotransformation metabolism) of B(*a*)P seemed to be slower than uptake, resulting in a net B(*a*)P bioaccumulation. For the same nominal B(*a*)P concentration used in the present study (100 μg/L; measured actual concentration 5 min after dosing 29.44 ± 4.58 μg/L), previous studies have also reported an up-regulation of *cyp1a* and induction of EROD activity in the liver of zebrafish exposed for 7 days, when a peak in the induction of these parameters is expected in teleosts (Thompson et al., 2010). This response was not observed in the gills. On the other hand, exposure to GO alone did not alter liver biotransformation metabolism (*cyp1a* or EROD) at any exposure time. Other works, however, have reported that a high concentration of rGO quantum dots (100 mg/L) significantly up-regulated *cyp1a*, through interaction with the AhR pathway in zebrafish embryos (J.H. Zhang et al., 2017). Apart from differences in exposure concentrations, effects produced by different graphene derivatives can differ completely depending on the surface characteristics of each NM (Guo and Mei, 2014; Jia et al., 2019), being the oxygen content on the surface one of the potential driving factors. When carbon NMs were combined with PAHs in the present study, the observed ability of B(*a*)P alone exposure to induce *cyp1a* and EROD in fish liver was not observed in fish exposed to GO with sorbed B(*a*)P. The lack of response of PAH exposure biomarkers in fish exposed to GO-B(*a*)P could be due to the lower level of exposure to B(*a*)P when sorbed to GO, as was reported for other carbon NMs in combination with PAHs (Della Torre et al., 2017) as well as consequent lower bioavailability and bioaccumulation. Similarly, the level of PAH exposure achieved in the GO + WAF treatment did not result enough to regulate the *cyp1a* transcription levels in zebrafish liver. According to Salaberria et al. (2014), a 50% WAF (1:40 North Sea crude oil/water), with a PAH content similar to that of the WAF used herein, was needed to cause *cyp1a* up-regulation in zebrafish liver after 24 and 72 h of exposure.

The transcription levels of liver *gstp1*, analysed as a key gene of phase II biotransformation metabolism, did not show significant changes in any treated group. Nevertheless, liver GST activity in fish exposed to B(*a*)P for 21 days presented a significant induction compared to GO-B(*a*)P exposed fishes. Whereas, Thompson et al. (2010) did not report induction of GST liver activity in zebrafish exposed to B(*a*)P for 7 days, exposure of red tilapia to 300 μg/L B(*a*)P for 10 days resulted in liver GST induction (Rodrigues et al., 2015). The presence of GO could inhibit the effect on liver GST activity induced by B(*a*)P exposure. Exposure to GO (1, 5 and 10 mg/L) has been reported to reduce the levels of glutathione (GSH), the co-factor of GST closely related with its activity (M. Chen et al., 2016), which could lead to the inhibition of GST activity (Glisic et al., 2015; M. Chen et al., 2016). On the contrary, GST activity was significantly induced in gills of fishes exposed for 3 days to GO + WAF and for 21 days to GO-B(*a*)P compared to fish exposed to GO, which showed the lowest gill GST activity among all treated fish. An inhibition of GST activity in gills was also observed in zebrafish after 48 h of injection of 50 mg/L of graphene (Fernandes et al., 2018). The fact that GST activity was induced significantly in gills of fish exposed to GO combined with PAHs (GO-B(*a*)P and GO + WAF), while the same response was not observed in the liver, suggests that the principal uptake route for these PAHs associated to GO could be through the gills. The contaminated GO (particulate) can directly impact on gills that are directly exposed to the water column and accumulate released PAHs as it has been demonstrated for other PAHs adsorbed on suspended particles (Zhai et al., 2020).

Analysis of *tp53* transcription levels in liver was carried out because of the involvement of this gene in cell cycle regulation. Its overexpression is considered a sign of protection against DNA damage that can trigger apoptosis or hepatocarcinogenesis in zebrafish (Lu et al., 2013). Metabolism of PAHs can lead to the formation of DNA damaging reactive intermediates (Storer and Zon, 2010). GO has been reported as an inducer of *tp53* in zebrafish embryos exposed to 50 mg/L of GO for 72 hpf (Jia et al., 2019). Regarding PAHs, no changes in the transcription levels of *tp53* were detected 14 days after injection of rainbow trout with 100 mg/kg of B(*a*)P (Phalen et al., 2017). In the present study, the *tp53* transcription levels were only significantly higher in fish exposed to GO-B(*a*)P compared to fish exposed to GO + WAF for 3 days, which presented the lowest values, and no significant differences were found compared to control fish, suggesting that the exposure concentrations were not high enough to induce DNA damage and to activate cell cycle regulation pathways.

Similarly, *cat*, *gpx1a* or *sod1* did not show any significant change among treatments, even though GO is known to affect antioxidant enzymes in zebrafish embryos as consequence of ROS generation (X. Zhang et al., 2017; Zou et al., 2018; Souza et al., 2019). Zou et al. (2018) reported an up-regulation of *gpx4b*, *sod2*, and *prdx1* in embryos exposed to 100 μg/L of GO. X. Zhang et al. (2017) also observed generation of ROS by 1–100 μg/L of GO with a consequent oxidative stress reflected by the significant increase of malondialdehyde content in GO exposed zebrafish. To the best of our knowledge, no previous works have reported effects in the transcription levels of oxidative stress-related genes caused by GO in adult zebrafish liver, but zebrafish embryos are expected to be more sensitive to GO compared with adult individuals. Accordingly, no significant effects were observed in liver CAT activity, which showed only significant differences in gills. All exposed fish presented higher CAT activity than controls, being significant in fish exposed to GO-B(*a*)P and B(*a*)P for 3 days and to GO + WAF for 21 days. Souza et al. (2019) reported induction of CAT activity in

zebrafish gills exposed to 2, 10 and 20 mg/L of GO for 48 h. This early response of the antioxidant system of zebrafish was reduced after 168 h of recovery in clean water. Other carbon NMs, such as C_{60} (20 mg/L), combined with B(*a*)P (8 μg/L), or B(*a*)P alone (8 μg/L) provoked a reduction of CAT activity in zebrafish embryos, while C_{60} alone produced induction of CAT (Della Torre et al., 2018).

AChE, that regulates the activity of acetylcholine, an important neurotransmitter involved in synaptic transmission of nerve impulses, was inhibited in all fish exposed for 21 days compared to control fish, but not in fish exposed for three days except in the case of the GO + WAF group. Hu et al. (2017) demonstrated that for a range of GO concentrations (0.01–1 μg/L), GO translocated to the brain of adult zebrafish and of their offspring with a subsequent inhibition of AChE activity in the offspring of exposed adults. AChE has also been typically reported to be altered in fish by xenobiotics, such as pesticides and PAHs (Holth and Tollefsen, 2012; Vieira et al., 2008; Kim et al., 2018). Phenanthrene, a common PAH present in most WAFs of crude oil, inhibited AChE activity in the head of adult zebrafish after 96 h of exposure to 750 μg/L (Kim et al., 2018). Another freshwater fish, *Electrophorus electricus*, showed inhibition of AChE after exposure to the produced water effluents from oil production platforms in the North Sea, being the aromatic PAHs, and not the polar and aliphatic fractions responsible of AChE inhibition (Holth and Tollefsen, 2012). In the common goby, exposure to 2 to 16 μg/L of B(*a*)P for 96 h also caused inhibition of AChE (Vieira et al., 2008).

Regarding histopathological alterations, a significant increase in the prevalence of liver vacuolisation was observed in fish exposed to GO + WAF for 3 and 21 days. Previous works observed 71.4% and 80% liver vacuolisation in zebrafish exposed to 2 mg/L and 20 mg/L of GO, respectively, for 14 days (M. Chen et al., 2016; Souza et al., 2017), but this was not observed in the present work. WAF from naphthenic crude oils have also been reported as disruptors of hepatic tissue. Agamy (2012) found the presence of lipid droplets in the liver of juvenile rabbit fish (*Siganus canaliculatus*) after 15 days and less frequently after 21 days of exposure to WAF. Co-exposure to GO + WAF PAHs, as in the present study, might increase the prevalence of hepatic pathologies compared to the effect of each treatment alone. Regarding gill tissues, none of the treatments of our study produced any significant histopathological alteration. Other studies did neither report remarkable effects on zebrafish gill tissue after exposure to GO at the same concentration used herein (M. Chen et al., 2016; Souza et al., 2017). Only at exposures from 10 to 20 mg/L of GO, gills of zebrafish presented some pathologies, such as lamellar fusion, clubbed tips, swollen mucocytes, epithelial lifting, aneurysms, and necrosis and these effects were closely related to ROS production due to GO exposure (Souza et al., 2017).

In summary, GO presented a high sorption capacity for PAHs that was driven mainly by the hydrophobicity of each PAH. Thus, GO in the environment could play a potential role as carrier of organic pollutants to aquatic organisms. Environmentally relevant concentrations of GO and rGO(PVP) did not cause significant effects on zebrafish embryo development (EC_{50} > 10 mg/L), even when they were combined with PAHs. Regarding sublethal effects in adult zebrafish, some evidences of toxicity were observed according to the results of catalase activity in zebrafish gills, but without further appearance of histopathological alterations in the gill tissue. The inhibition of AChE activity in all fish treated for 21 days indicated a potential neurotoxic effect. Only dissolved B(*a*)P provoked changes in liver biotransformation biomarkers, even at gene level, and these effects were reduced when zebrafish were exposed to GO combined with PAHs. At tissue level, hepatic vacuolisation was observed in fish co-exposed to GO + WAF, which is possibly linked to the bioavailability of the PAHs from WAF when they are associated with GO. Taken together, the results suggested that graphene oxide NMs, alone and in combination with PAHs, are a potential source of toxicity to fish, but at concentrations that are currently above the expected environmental levels.

CRediT authorship contribution statement

Ignacio Martínez-Álvarez: Methodology, Formal analysis, Investigation, Writing – original draft, Visualization. **Karyn Le Menach:** Methodology, Validation, Investigation, Resources. **Marie-Hélène Devier:** Resources. **Iranzu Barbarin:** Resources. **Radmila Tomovska:** Resources, Writing – review & editing. **Miren P. Cajaraville:** Conceptualization, Writing – review & editing, Project administration, Funding acquisition. **Hélène Budzinski:** Conceptualization, Validation, Writing – review & editing, Supervision, Project administration, Funding acquisition. **Amaia Orbea:** Conceptualization, Validation, Resources, Writing – review & editing, Visualization, Supervision, Project administration, Funding acquisition.

Declaration of competing interest

The authors declare that they have no known competing financial interests or personal relationships that could have appeared to influence the work reported in this paper.

Acknowledgments

This work has been funded by University of the Basque Country (predoctoral grant to IMA PIFBUR15/15), Basque Government (consolidated research group IT810-13 and IT1302-19), Spanish Ministry of Economy and Competitiveness project NACE (CTM2016-81130-R), French National Research Agency (No.–10–IDEX-03-02) and Cluster of Excellence Continental To coastal Ecosystems-COTE (ANR-10-LABX 45). Thanks to staff at Driftslaboratoriet Mongstad, Equinor (former Statoil) for supplying the sample of crude oil used in the experiments. The authors thank for technical and human support provided by SGIker (UPV/EHU/ERDF, EU). The authors gratefully acknowledge to Dr. José M. Lacave and to Julián García for help with the experimental set up and support in sample preparation and processing.

Appendix A. Supplementary data

Supplementary data to this article can be found online at https://doi.org/10.1016/j.scitotenv.2021.145669.

References

Aebi, H., 1984. Catalase in vitro. Meth. Enzymol. 105, 121–126.
Agamy, E., 2012. Histopathological liver alterations in juvenile rabbit fish (*Siganus canaliculatus*) exposed to light Arabian crude oil, dispersed oil and dispersant. Ecotox. Environ. Safe. 75, 171–179.
Apul, O.G., Wang, Q., Zhou, Y., Karanfil, T., 2013. Adsorption of aromatic organic contaminants by graphene nanosheets: comparison with carbon nanotubes and activated carbon. Water Res. 47, 1648–1654.
Baig, N., Ihsanullah, Sajid, M., Saleh, T.A., 2019. Graphene-based adsorbents for the removal of toxic organic pollutants: a review. J. Environ. Manag. 244, 370–382.
Baumard, P., Budzinski, H., Garrigues, P., 1997. Analytical procedure for the analysis of PAHs in biological tissues by gas chromatography coupled to mass spectrometry: application to mussels. Fresenius J. Anal. Chem. 359, 502–509.
Baumard, P., Budzinski, H., Garrigues, P., Dizer, H., Hansen, P.D., 1999. Polycyclic aromatic hydrocarbons in recent sediments and mussels (*Mytilus edulis*) from the Western Baltic Sea: occurrence, bioavailability and seasonal variations. Mar. Environ. Res. 47, 17–47.
Brand, M., Granato, M., Nüsslein-Volhard, C., 2002. Chapter 1: keeping and raising zebrafish. In: Nusslein-Volhard, C., Dahm, R. (Eds.), Zebrafish: A Practical Approach. Oxford University Press, New York, pp. 7–37.
Carter, M.C., Kilduff, J.E., Weber Jr., W.J., 1995. Site energy distribution analysis of preloaded adsorbents. Environ. Sci. Technol. 29, 1773–1780.
Castro, V.L., Clemente, Z., Jonsson, C., Silva, M., Vallim, J.H., de Medeiros, A.M.Z., Martinez, D.S.T., 2018. Nanoecotoxicity assessment of graphene oxide and its relationship with humic acid: Nanoecotoxicity of graphene oxide and humic acid. Environ. Toxicol. Chem. 37, 1998–2012.
ChemIDplus by SRC, Inc, 2020. http://chem.sis.nlm.nih.gov/chemidplus/name/benzo(a)pyrene. (Accessed 20 January 2020).
Chen, L., Hernandez, Y., Feng, X., Müllen, K., 2012. From nanographene and graphene nanoribbons to graphene sheets: chemical synthesis. Angew. Chem. Int. Ed. 51, 764–7654.

Chen, M., Yin, J., Liang, Y., Yuan, S., Wang, F., Song, M., Wang, H., 2016a. Oxidative stress and immunotoxicity induced by graphene oxide in zebrafish. Aquat. Toxicol. 174, 54–60.
Chen, Y., Hu, X., Sun, J., Zhou, Q., 2016b. Specific nanotoxicity of graphene oxide during zebrafish embryogenesis. Nanotoxicology 1–11.
Chowdhury, I., Duch, M.C., Mansukhani, N.D., Hersam, M.C., Bouchard, D., 2013. Colloidal properties and stability of graphene oxide nanomaterials in the aquatic environment. Environ. Sci. Technol. 47, 6288–6296.
Ciriminna, R., Zhang, N., Yang, M., Meneguzzo, F., Xu, Y., Pagliaro, M., 2015. Commercialization of graphene-based technologies: a critical insight. Chem. Comm. 51, 7090–7095.
D'Amora, M., Camisasca, A., Lettieri, S., Giordani, S., 2017. Toxicity assessment of carbon nanomaterials in zebrafish during development. Nanomaterials 7, 414.
Dasmahapatra, A.K., Dasari, T.P.S., Tchounwou, P.B., 2019. Graphene-based nanomaterials toxicity in fish. In: de Voogt, P. (Ed.), Reviews of Environmental Contamination and Toxicology. volume 247. Springer International Publishing, Cham, pp. 1–58.
De Marchi, L., Pretti, C., Gabriel, B., Marques, P.A.A.P., Freitas, R., Neto, V., 2018. An overview of graphene materials: properties, applications and toxicity on aquatic environments. Sci. Total Environ. 631-632, 1440–1456.
Della Torre, C., Parolini, M., Del Giacco, L., Ghilardi, A., Ascagni, M., Santo, N., Maggioni, D., Magni, S., Madaschi, L., Prosperi, L., La Porta, C., Binelli, A., 2017. Adsorption of B(α)P on carbon nanopowder affects accumulation and toxicity in zebrafish (*Danio rerio*) embryos. Environ. Sci. Nano 4, 1132–1146.
Della Torre, C., Maggioni, D., Ghilardi, A., Parolini, M., Santo, N., Landi, C., Madaschi, L., Magni, S., Tasselli, S., Ascagni, M., Bini, L., La Porta, C., Del Giacco, L., Binelli, A., 2018. The interactions of fullerene C60 and Benzo(α)pyrene influence their bioavailability and toxicity to zebrafish embryos. Environ. Pollut. 241, 999–1008.
Ellman, G.L., Courtney, K.D., Andres, V., Featherstone, R.M., 1961. A new and rapid colorimetric determination of acetylcholinesterase activity. Biochem. Pharmacol. 7, 88–90.
Fako, V.E., Furgeson, D.Y., 2009. Zebrafish as a correlative and predictive model for assessing biomaterial nanotoxicity. Adv. Drug Deliv. Rev. 61, 478–486.
Falconer, J.L., Jones, C.F., Lu, S., Grainger, D.W., 2015. Carbon nanomaterials rescue phenanthrene toxicity in zebrafish embryo cultures. Environ. Sci. Nano 2, 645–652.
Fernandes, A.L., Nascimento, J.P., Santos, A.P., Furtado, C.A., Romano, L.A., Eduardo da Rosa, C., Monserrat, J.M., Ventura-Lima, J., 2018. Assessment of the effects of graphene exposure in *Danio rerio*: a molecular, biochemical and histological approach to investigating mechanisms of toxicity. Chemosphere 210, 458–466.
Forth, H.P., Mitchelmore, C.L., Morris, J.M., Lipton, J., 2017. Characterization of oil and water accommodated fractions used to conduct aquatic toxicity testing in support of the Deepwater Horizon oil spill natural resource damage assessment. Environ. Toxicol. Chem. 36, 1450–1459.
Ghosal, K., Sarkar, K., 2018. Biomedical applications of graphene nanomaterials and beyond. ACS Biomater. Sci. Eng. 4, 2653–2703.
Glisic, B., Mihaljevic, I., Popovic, M., Zaja, R., Loncar, J., Fent, K., Kovacevic, R., Smital, T., 2015. Characterization of glutathione-S-transferases in zebrafish (*Danio rerio*). Aquat. Toxicol. 158, 50–62.
Guo, X., Mei, N., 2014. Assessment of the toxic potential of graphene family nanomaterials. J. Food Drug Anal. 22, 105–115.
Habig, W.H., Jakoby, W.B., 1981. Assays for differentiation of glutathione S-transferases. Methods Enzymol. 77, 398–405.
Holth, T.F., Tollefsen, K.E., 2012. Acetylcholine esterase inhibitors in effluents from oil production platforms in the North Sea. Aquat. Toxicol. 112–113, 92–98.
Hu, X., Wei, Z., Mu, L., 2017. Graphene oxide nanosheets at trace concentrations elicit neurotoxicity in the offspring of zebrafish. Carbon 117, 182–191.
Ji, L., Chen, W., Xu, Z., Zheng, S., Zhu, D., 2013. Graphene nanosheets and graphite oxide as promising adsorbents for removal of organic contaminants from aqueous solution. J. Environ. Qual. 42, 191–198.
Jia, P.-P., Sun, T., Junaid, M., Yang, L., Ma, Y.-B., Cui, Z.-S., Wei, D.-P., Shi, H.-F., Pei, D.-S., 2019. Nanotoxicity of different sizes of graphene (G) and graphene oxide (GO) in vitro and in vivo. Environ. Pollut. 247, 595–606.
Katsumiti, A., Tomovska, R., Cajaraville, M.P., 2017. Intracellular localization and toxicity of graphene oxide and reduced graphene oxide nanoplatelets to mussel hemocytes in vitro. Aquat. Toxicol. 188, 138–147.
Kennedy, S.W., Jones, S.P., 1994. Simultaneous measurement of cytochrome P4501A catalytic activity and total protein concentration with a fluorescence plate reader. Anal. Biochem. 222 (1), 217–223.
Kim, K., Jeon, H., Choi, S., Tsang, D.C.W., Oleszczuk, P., Ok, Y.S., Lee, H., Lee, S., 2018. Combined toxicity of endosulfan and phenanthrene mixtures and induced molecular changes in adult zebrafish (*Danio rerio*). Chemosphere 194, 30–41.
Kinloch, I.A., Suhr, J., Lou, J., Young, R.J., Ajayan, P.M., 2018. Composites with carbon nanotubes and graphene: an outlook. Science 362, 547–553.
Kong, W., Kum, H., Bae, S., Shim, J., Kim, H., Kong, L., Meng, Y., Wang, K., Kim, C., Kim, J., 2019. Path towards graphene commercialization from lab to market. Nat. Nanotechnol. 14, 927–938.
Lacave, J.M., Fanjul, A., Bilbao, E., Gutierrez, N., Barrio, I., Arostegui, I., Cajaraville, M.P., Orbea, A., 2017. Acute toxicity, bioaccumulation and effects of dietary transfer of silver from brine shrimp exposed to PVP/PEI-coated silver nanoparticles to zebrafish. Comp. Biochem. Physiol. Part C 199, 69–80.
Lacave, J.M., Vicario-Parés, U., Bilbao, E., Gilliland, D., Mura, F., Dini, L., Cajaraville, M.P., Orbea, A., 2018. Waterborne exposure of adult zebrafish to silver nanoparticles and to ionic silver results in differential silver accumulation and effects at cellular and molecular levels. Sci. Total Environ. 642, 1209–1220.
Lammel, T., Navas, J.M., 2014. Graphene nanoplatelets spontaneously translocate into the cytosol and physically interact with cellular organelles in the fish cell line PLHC-1. Aquat. Toxicol. 150, 55–65.
Lammel, T., Boisseaux, P., Navas, J.M., 2014. Potentiating effect of graphene nanomaterials on aromatic environmental pollutant-induced cytochrome P450 1A expression in the topminnow fish hepatoma cell line PLHC-1. Environ. Toxicol. 30, 1192–1204.
Li, B., Ou, P., Wei, Y., Zhang, X., Song, J., 2018. Polycyclic aromatic hydrocarbons adsorption onto graphene: a DFT and AIMD study. Materials 11, 726.
Linard, E.N., Apul, O.G., Karanfil, T., van den Hurk, P., Klaine, S.J., 2017. Bioavailability carbon nanomaterial-adsorbed polycyclic aromatic hydrocarbons to *Pimephales promelas*: influence of adsorbate molecular size and configuration. Environ. Sci. Technol. 51, 9288–9296.
Liu, X.T., Mu, X.Y., Wu, X.L., Meng, L.X., Guan, W.B., Ma, Y.Q., Sun, H., Wang, C.J., Li, X.F., 2014. Toxicity of multi-walled carbon nanotubes, graphene oxide, and reduced graphene oxide to zebrafish embryos. Biomed. Environ. Sci. 27 (9), 676–683.
Liu, Y., Bai, J., Yao, H., Li, G., Zhang, T., Li, S., Zhang, L., Si, J., Zhou, R., Zhang, H., 2020. Embryotoxicity assessment and efficient removal of naphthalene from water by irradiated graphene aerogels. Ecotoxicol. Environ. Saf. 189, 110051.
Livak, K.J., Schmittgen, T.D., 2001. Analysis of relative gene expression data using real-time quantitative PCR and the $2-\Delta\Delta CT$ method. Methods 25, 402–408.
Livingstone, D.R., 1998. The fate of organic xenobiotics in aquatic ecosystems: quantitative and qualitative differences in biotransformation by invertebrates and fish. Comp. Biochem. Physiol. Part A 120, 43–49.
Lu, J., Yang, W., Tsai, S., Lin, Y., Chang, P., Chen, J., Wang, H., Wu, J., Jin, S.C., Yuh, C., 2013. Liver-specific expressions of HBx and src in the p53 mutant trigger hepatocarcinogenesis in zebrafish. PLoS One 8, e76951.
Luque-Alled, J.M., Abdel-Karim, A., Alberto, M., Leaper, S., Perez-Page, M., Huang, K., Vijayaraghavan, A., El-Kalliny, A.S., Holmes, S.M., Gorgojo, P., 2020. Polyethersulfone membranes: from ultrafiltration to nanofiltration via the incorporation of APTS functionalized-graphene oxide. Sep. Purif. Technol. 230, 115836.
Naasz, S., Altenburger, R., Kühnel, D., 2018. Environmental mixtures of nanomaterials and chemicals: the Trojan-horse phenomenon and its relevance for ecotoxicity. Sci. Total Environ. 635, 1170–1181.
Niu, Z., Liu, L., Zhang, L., Chen, X., 2014. Porous graphene materials for water remediation. Small 10, 3434–3441.
OECD TG236, 2013. OECD guidelines for the testing of chemicals. Section 2: Effects on Biotic Systems Test No. 236: Fish Embryo Acute Toxicity (FET) Test. Organization for Economic Cooperation and Development, Paris, France (22 pp.).
Orbea, A., González-Soto, N., Lacave, J.M., Barrio, I., Cajaraville, M.P., 2017. Developmental and reproductive toxicity of PVP/PEI-coated silver nanoparticles to zebrafish. Comp. Biochem. Physiol. Part C: Toxicol. Pharmacol. 199, 59–68.
Pecoraro, R., D'Angelo, D., Filice, S., Scalese, S., Capparucci, F., Marino, F., Iaria, C., Guerriero, G., Tibullo, D., Scalisi, E.M., Salvaggio, A., Nicotera, I., Brundo, M.V., 2018. Toxicity evaluation of graphene oxide and titania loaded nafion membranes in zebrafish. Front. Physiol. 8, 1039.
Pei, Z., Li, L., Sun, L., Zhang, S., Shan, X., Yang, S., Wen, B., 2013. Adsorption characteristics of 1,2,4-trichlorobenzene, 2,4,6-trichlorophenol, 2-naphthol and naphthalene on graphene and graphene oxide. Carbon 51, 156–163.
Phalen, L.J., Köllner, B., Hogan, N.S., van den Heuvel, M.R., 2017. Transcriptional response in rainbow trout (*Oncorhynchus mykiss*) B cells and thrombocytes following in vivo exposure to benzo[a]pyrene. Environ. Toxicol. Pharmacol. 53, 212–218.
Ren, C., Hu, X., Li, X., Zhou, Q., 2016. Ultra-trace graphene oxide in a water environment triggers Parkinson's disease-like symptoms and metabolic disturbance in zebrafish larvae. Biomaterials 93, 83–94.
Rodrigues, A.F.C., Moneró, T.O., Frighetto, R.T.S., de Almeida, E.A., 2015. E2 potentializes benzo(a)pyrene-induced hepatic cytochrome P450 enzyme activities in Nile tilapia at high concentrations. Environ. Sci. Pollut. Res. 22, 17367–17374.
Salaberria, I., Brakstad, O.G., Olsen, A.J., Nordtug, T., Hansen, B.H., 2014. Endocrine and AhR-CYP1A pathway responses to the water-soluble fraction of oil in zebrafish (*Danio rerio* Hamilton). J. Toxicol. Environ. Health, Part A 77, 506–515.
Salazar-Coria, L., Rocha-Gómez, M.A., Matadamas-Martínez, F., Yépez-Mulia, L., Vega-López, A., 2019. Proteomic analysis of oxidized proteins in the brain and liver of the Nile tilapia (*Oreochromis niloticus*) exposed to a water-accommodated fraction of Maya crude oil. Ecotoxicol. Environ. Saf. 17, 609–620.
Singer, M.M., Aurand, D., Bragins, G.E., Clark, J.R., Coelho, G.M., Sowby, M.L., Tjeerdema, R.S., 2000. Standardization of the preparation and quantitation of water-accommodated fractions of petroleum for toxicity testing. Mar. Pollut. Bull. 40, 1007–1016.
Smith, S.C., Rodrigues, D.F., 2015. Carbon-based nanomaterials for removal of chemical and biological contaminants from water: a review of mechanisms and applications. Carbon 91, 122–143.
Soares, J., Pereira, T., Costa, K., Maraschin, T., Basso, N., Bogo, M., 2017. Developmental neurotoxic effects of graphene oxide exposure in zebrafish larvae (*Danio rerio*). Colloids Surf. B Biointerfaces 157, 335–346.
Souza, J.P., Baretta, J.F., Santos, F., Paino, I.M.M., Zucolotto, V., 2017. Toxicological effects of graphene oxide on adult zebrafish (*Danio rerio*). Aquat. Toxicol. 186, 11–18.
Souza, J.P., Mansano, A.S., Venturini, F.P., Santos, F., Zucolotto, V., 2019. Antioxidant metabolism of zebrafish after sub-lethal exposure to graphene oxide and recovery. Fish. Physiol. Biochem. 45, 1289–1297.
Statoil, 2011. Crude summary report. Available at:. https://www.statoil.com/content/dam/statoil/documents/crude-oil-assays/Statoil-TROLL-BLEND-2011-01.xls. (Accessed November 2018).
Storer, N.Y., Zon, L.I., 2010. Zebrafish models of p53 functions. Cold Spring Harb. Perspect. Med. 2, a001123.
Sun, Y., Yang, S., Zhao, G., Wang, Q., Wang, X., 2013. Adsorption of polycyclic aromatic hydrocarbons on graphene oxides and reduced graphene oxides. Chem. Asian J. 8, 2755–2761.

Tabish, T.A., Memon, F.A., Gomez, D.E., Horsell, D.W., Zhang, S., 2018. A facile synthesis of porous graphene for efficient water and wastewater treatment. Sci. Rep. 8, 1817–1831.
Thompson, E.D., Burwinkel, K.E., Chava, A.K., Notch, E.G., Mayer, G.D., 2010. Activity of phase I and phase II enzymes of the benzo[a]pyrene transformation pathway in zebrafish (*Danio rerio*) following waterborne exposure to arsenite. Comp. Biochem. Physiol. Part C: Toxicol. Pharmacol. 152, 371–378.
Turja, R., Soirinsuo, A., Budzinski, H., Devier, M.H., Lehtonen, K.K., 2013. Biomarker responses and accumulation of hazardous substances in mussels (*Mytilus trossulus*) transplanted along a pollution gradient close to an oil terminal in the Gulf of Finland (Baltic Sea). Comp. Biochem. Physiol. Part C: Toxicol. Pharmacol. 157, 80–92.
Turja, R., Höher, N., Snoejis, P., Baršienė, J., Butrimavičienė, L., Kuznetsova, T., Kholodkevich, S.V., Devier, M.H., Budzinski, H., Lehtonen, K.K., 2014. A multibiomarker approach to the assessment of pollution impacts in two Baltic Sea coastal areas in Sweden using caged mussels (*Mytilus trossulus*). Sci. Total Environ. 473, 398–409.
Velki, M., Meyer-Alert, H., Seiler, T.-B., Hollert, H., 2017. Enzymatic activity and gene expression changes in zebrafish embryos and larvae exposed to pesticides diazinon and diuron. Aquat. Toxicol. 193, 187–200.
Vieira, L.R., Sousa, A., Frasco, M.F., Lima, I., Morgado, F., Guilhermino, L., 2008. Acute effects of Benzo[a]pyrene, anthracene and a fuel oil on biomarkers of the common goby *Pomatoschistus microps* (Teleostei, Gobiidae). Sci. Total Environ. 395, 87–100.
Wang, J., Chen, B., 2015. Adsorption and coadsorption of organic pollutants and a heavy metal by graphene oxide and reduced graphene materials. Chem. Eng. J. 281, 379–388.
Wang, Y., Li, Z., Wang, J., Li, J., Lin, Y., 2011. Graphene and graphene oxide: biofunctionalization and applications in biotechnology. Trends Biotechnol. 29, 205–212.
Wang, J., Chen, Z., Chen, B., 2014. Adsorption of polycyclic aromatic hydrocarbons by graphene and graphene oxide nanosheets. Environ. Sci. Technol. 48, 4817–4825.
Yan, H., Wu, H., Li, K., Wang, Y., Tao, X., Yang, H., Li, A., Cheng, R., 2015. Influence of the surface structure of graphene oxide on the adsorption of aromatic organic compounds from water. Appl. Mater. Interfaces 7, 6690–6697.
Yan, J., Chen, L., Huang, C., Lung, S.C., Yang, L., Wang, W., Lin, P., Suo, G., Lin, C., 2017. Consecutive evaluation of graphene oxide and reduced graphene oxide nanoplatelets immunotoxicity on monocytes. Colloids Surf. B: Biointerfaces 153, 300–309.
Yang, J., Zhong, W., Chen, P., Zhang, Y., Sun, B., Liu, M., Zhu, Y., Zhu, L., 2019a. Graphene oxide mitigates endocrine disruption effects of bisphenol A on zebrafish at an early development stage. Sci. Total Environ. 697, 134158.
Yang, Z., Yang, Q., Zheng, G., Han, S., Zhao, F., Hu, Q., Fu, Z., 2019b. Developmental neurotoxicity and immunotoxicity induced by graphene oxide in zebrafish embryos. Environ. Toxicol. 34, 415–423.
Zhai, Y., Xia, X., Wang, H., Lin, H., 2020. Effect of suspended particles with different grain sizes on the bioaccumulation of PAHs by zebrafish (*Danio rerio*). Chemosphere 242, 125299.
Zhang, J., Shen, G., Wang, W., Zhou, X., Guo, S., 2010. Individual nanocomposite sheets of chemically reduced graphene oxide and poly(N-vinyl pyrrolidone): preparation and humidity sensing characteristics. J. Mater. Chem. 20, 10824.
Zhang, J.-H., Sun, T., Niu, A., Tang, Y.-M., Deng, S., Luo, W., Xu, Q., Wei, D., Pei, D.-S., 2017a. Perturbation effect of reduced graphene oxide quantum dots (rGOQDs) on aryl hydrocarbon receptor (AhR) pathway in zebrafish. Biomaterials 133, 49–59.
Zhang, X., Zhou, Q., Zou, W., Hu, X., 2017b. Molecular mechanisms of developmental toxicity induced by graphene oxide at predicted environmental concentrations. Environ. Sci. Technol. 51, 7861–7871.
Zhao, Y., Luo, K., Fan, Z., Huang, C., Hu, J., 2013. Modulation of benzo[a]pyrene-induced toxic effects in japanese medaka (*Oryzias latipes*) by 2,2′,4,4′-tetrabromodiphenyl ether. Environ. Sci. Techno. 47, 13068–13076.
Zhao, J., Wang, Z., Zhao, Q., Xing, B., 2014. Adsorption of phenanthrene on multilayer graphene as affected by surfactant and exfoliation. Environ. Sci. Technol. 48, 331–339.
Zou, W., Zhou, Q., Zhang, X., Mu, L., Hu, X., 2018. Characterization of the effects of trace concentrations of graphene oxide on zebrafish larvae through proteomic and standard methods. Ecotoxicol. Environ. Saf. 159, 221–231.